Static and Dynamic Electronic Spectroscopy at Liquid Interfaces

Ilan Benjamin

Department of Chemistry, University of California, Santa Cruz, California 95064

Received May 3, 2005

Contents

Ilan Benjamin was born in Israel in 1956. He received his B.Sc. in chemistry and physics from the Hebrew University of Jerusalem in 1982 and his Ph.D. in theoretical chemistry in 1986, working under the direction of Professor Raphael Levine at the Hebrew University of Jerusalem. He was a Weizmann Postdoctoral Fellow at the University of Pennsylvania and also held a postdoctoral position at the University of California at San Diego. In 1989, he joined the faculty at the University of California at Santa Cruz, where he is currently a Professor of physical chemistry. In 1995–1996, he was a visiting professor at the Weizmann Institute of Science, Israel. Benjamin's research interests include the theoretical and computational studies of relaxation processes and chemical reaction dynamics in the condensed phase. In recent years, his research has focused on chemical reactions and molecular interactions at liquid interfaces.

1. Introduction and Scope

Many important and fundamental processes in science and technology take place at liquid interfaces. Examples include uptake and reactions of pollutants at the surface of water droplets and ice particles in the atmosphere,[1,2] phase transfer catalysis,[3−5] ion-, electron-, and proton-transfer reactions at liquid/liquid and liquid/membrane interfaces,[6−8] and corrosion.[9,10] While the study of these systems has a very long history, up until recently most of the experimental studies involved the measurements of bulk macroscopic properties, and most of the theoretical studies utilized continuum models.[11] In recent years, due to progress in experimental and theoretical methodology, it has become clear that the study of the molecular structure and dynamics of liquid interfaces is an important step toward understanding the role that this inhomogeneous environment plays in the phenomena listed above.

Static and dynamic electronic spectroscopy has been used for several decades to gain insight into the nature of intermolecular interactions, structure, and dynamics in condensed media.[12−57] With the development of nonlinear optical spectroscopic techniques,[58] these tools have been utilized, primarily in the past decade, to study liquid interfaces. The purpose of this paper is to review the progress made in the application of electronic spectroscopy to liquid interfaces. This subject has been previously reviewed briefly.[59−61] However, major contributions, primarily during the last 5−7 years, justify a more comprehensive review of this topic.

We begin this paper (sections 2.1 and 2.2) with an exposition of the basic theoretical background underlying the phenomena of static and dynamic electronic spectroscopy in the condensed phase. This part is a necessary background, especially when the results at liquid interfaces are to be compared with the bulk. However, given its extensive coverage in the literature, this part will be brief, and for additional details, the reader is directed to existing literature. This is followed (in section 2.3) with a summary of the most important knowledge gained in the past decade about the structure and dynamics of the neat interface, which is

10.1021/cr040362f CCC: $59.00
Published on Web 02/07/2006

essential background for the rest of the paper. However, it will be limited to a brief summary. More details are available in a number of reviews, which are listed there.

The rest of the paper contains a review of the applications to liquid/vapor and liquid/liquid interfaces. Because some of the characteristics of liquid/liquid interfaces are similar to those in bulk micelle solutions (including reverse micelles and microemulsions) and at liquid/solid interfaces, some discussion of these systems for comparison purposes is included here, but no exhaustive review was attempted, because there are relatively recent reviews of these systems.[57,62] While an attempt has been made to review all of the pertinent literature, the emphasis is on the theoretical literature and on the microscopic insight. Since most of what is known theoretically has been obtained by computer simulations, the review will be heavily biased toward results obtained using this technique. Several reviews in this thematic issue address some of the material covered here from the experimental point of view. Technical details about the computations and the potential energy surfaces will be kept to a minimum, and the reader will be directed toward the specific papers. Finally, our emphasis is on the general effect of the inhomogeneous environment and a comparison with the bulk, rather than on the specifics of a given interfacial system.

2. Background

In this section, we briefly discuss some of the background required to follow the main parts of this paper. No attempt has been made to provide an exhaustive review of the topics covered here, but rather we provide useful information in preparation for the detailed and full review of the main topics presented in sections 3 and 4.

2.1. Electronic Spectroscopy in the Condensed Phase

The line shape of an electronic absorption and emission spectrum of a dilute solute in a solvent is typically broader and its peak shifts compared with the spectrum in the gas phase. The shift of the spectrum reflects the different interaction energies between the ground and excited states of the solute with the solvent. The width reflects the (mainly) orientational distribution and the fluctuations of solvent molecules. Clearly, solvent effects on electronic spectra contain valuable information about solvent structure in the vicinity of the solute and about solvent−solute interactions. This information is critically important for understanding solvent effects on chemical reactivity and thus has been the subject of numerous experimental and theoretical studies. In this section, we briefly present a simple model for the static absorption and emission spectra. In the next section, we will consider the time-dependent version.

We consider a single vibronic transition and model it by a two-level quantum system coupled to a classical bath. (For recent articles discussing the contribution of intramolecular solute vibration coupled to a semiclassical or quantum bath with extensive references to other earlier treatments, see refs 63 and 64.) We take H_{gr} and H_{ex} as the total Hamiltonian of the system when the solute is in the ground and excited electronic states, respectively. The energy difference between the two states is modified from the gas-phase value of E_0 because of the different interactions between the solvent and solute in the two electronic states. We denote by $U[\mathbf{r}] = H_{ex} - H_{gr}$ the energy gap at a particular nuclear configuration $\mathbf{r}$ (of the solute and all solvent molecules). In the dipole approximation for the interaction with the electromagnetic field (weak field), if one neglects solvent dynamics (see next section) and excited-state lifetime (assumed infinite), then in the Franck−Condon approximation the normalized absorption and emission static line shapes are given by the distribution of energy gaps in the ground and excited state, respectively (in units of $\hbar = 1$):

$$I_{abs}(\omega) = \langle \delta[\omega - U(\mathbf{r})] \rangle_{gr}$$
$$I_{emis}(\omega) = \langle \delta[\omega - U(\mathbf{r})] \rangle_{ex} \quad (2.1)$$

where δ is the Dirac δ function and $\langle ... \rangle_\alpha = \int e^{-\beta H_\alpha} ... d\mathbf{r} / (\int e^{-\beta H_\alpha} d\mathbf{r})$ represents the canonical ($\beta = 1/(kT)$) ensemble average when the system's Hamiltonian is H_α (α = gr or ex). Equation 2.1 is the basis for a classical computer simulation calculation of the line shape: One runs molecular dynamics or Monte Carlo simulations with the Hamiltonian H_{gr} (or H_{ex}) and bins the instantaneous energy gap to obtain the absorption (or emission) spectrum. This equation is also the starting point of several analytical (and combined analytical−simulation) theories of electronic line shape.

By replacement of the δ function with its Fourier representation, $\langle \delta(\omega - U) \rangle = (2\pi)^{-1} \int_{-\infty}^{\infty} e^{-i\omega t} \langle e^{iUt} \rangle dt$, and use of the second-order cumulant expansion of $\langle e^{iUt} \rangle$, it is straightforward to show that these line shapes are Gaussians whose peaks are given by $\omega_{abs} = \langle U \rangle_{gr}$ and $\omega_{emis} = \langle U \rangle_{ex}$ for the absorption and emission spectra, respectively:[29,40,65]

$$I_{abs}(\omega) = \frac{1}{\sqrt{2\pi\sigma_a^2}} e^{-(\omega - \langle U \rangle_{gr})^2/(2\sigma_a^2)}, \quad \sigma_a^2 = \langle U^2 \rangle_{gr} - \langle U \rangle_{gr}^2$$
$$I_{emis}(\omega) = \frac{1}{\sqrt{2\pi\sigma_e^2}} e^{-(\omega - \langle U \rangle_{ex})^2/(2\sigma_e^2)},$$
$$\sigma_e^2 = \langle U^2 \rangle_{ex} - \langle U \rangle_{ex}^2 \quad (2.2)$$

These results have been used to obtain approximate analytical formulas for the solvent-induced shift of the peak absorption and emission spectra. We mention a few examples of these results here for future use.

Using the Onsager reaction field model, McRae computed the spectral shift in terms of the solvent static dielectric constant and the index of refraction for a solute modeled as a point dipole inside a cavity and undergoing an excitation that involves a change in the dipole (size and orientation), as well as a change in the polarizability.[66] The resulting (quite lengthy) expression has been modified and applied by many authors to calculate excited electronic state solute properties.[28,67,68] For example, in the case of a point dipole in a nonpolarizable liquid and a parallel transition (no change in the dipole moment orientation upon excitation), the expression for the shift relative to the gas phase is reduced to

$$\Delta\omega = \frac{4\mu_{gr}(\mu_{gr} - \mu_{ex})}{R^3} \frac{\epsilon - 1}{\epsilon + 2} \quad (2.3)$$

where μ_{gr} and μ_{ex} are the electric dipole moments in the ground and excited states, respectively, and R is the radius of the cavity. This formula shows that if the excited-state

dipole is larger than the ground-state one (the excited state is stabilized more than the ground state), the spectrum is red-shifted, which is referred to as positive solvatochromism (sometimes called bathochromism). A blue shift (negative solvatochromism or hypsochromism) arises when $\mu_{ex} < \mu_{gr}$. Expressions for polarizable solvents, including practical applications, are given in ref 69. The shift can also be related to the thermodynamic properties of the system.[12,28] Statistical mechanical theories in which the solvent and the solvent−solute coupling are modeled using interaction potential models are also very extensive.[29,40,65,70,71] Particularly useful are those results that express the frequency shift and the width in terms of the solvent−solute radial distribution functions[29] (which can be obtained from simulations or approximate statistical mechanical theories). A test of continuum models was reported by Bader and Berne,[37] who suggested that one way to improve the results of continuum models (for polar−polarizable solvents) is to allow for a change in the cavity size upon excitation.

Especially relevant to our discussion of liquid interfaces is the empirically based approach to quantitatively expressing the differential solvation of the ground and excited states of a solute by introducing the concept of a solvent polarity scale.[72−75] The basic idea is that simple solvent properties such as dielectric constant and index of refraction are not sufficient to predict the ability of the solvent to solvate a polar solute, since that ability may depend on the details of the solvent−solute coupling and the solvent structure. In contrast, as the discussion above suggests, the electronic spectral shift provides a convenient one-parameter characterization of the ability of the solvent to interact with the solute. This has led to the development of several solvent polarity scales based on the spectral shift of several different dye molecules (referred to as solvent polarity indicators). The electronic transition used is typically the $\pi \rightarrow \pi^*$ transition in aromatic compounds. For example, one of the most useful scales, called the $E_T(30)$ scale, is based on pyridinium *N*-phenolate betaine dye. The spectral shift of this solute molecule in hundreds of different solvents was measured, and a convenient scale was produced by expressing the shift in kcalories per mole. Reichardt has compiled these values for many solvents and also compared a number of other polarity scales.[38]

The polarity scale expresses quantitatively the notion that as the solvent polarity increases, the solvatochromism increases for solute molecules that are similar to the indicator molecule used to set up the scale. This, however, assumes that change in the solvent does not affect the solute electronic structure, which is not always the case.[76,77] For example, if the ground state polarizability is especially large, a positive solvatochromism may switch to a negative one with an increase in solvent polarity.[38,78] An example of this at a liquid/liquid interface will be presented below.

We conclude this section with an important point that has been stressed in the literature.[38,79] Representing the solvation power of a liquid using a single parameter is reasonable if the solvent−solute interactions are nonspecific (such as dipolar interactions).[75] This, however, is not the case if there are specific types of interactions, such as hydrogen bonding. Thus, a multiparameter approach, in which additional parameters describe these specific interactions, can be introduced. An example is the Kamlet−Taft empirical approach, where in addition to the dipolar/polarizability parameter π^*, one introduces a parameter to describe hydrogen-bond donor acidity (α) and another parameter to describe hydrogen-bond acceptor basicity (β).[72,80,81] The success of such an approach depends on the ability to find indicator molecules that interact with the solvents primarily through the mechanism one tries to model. For a recent review with extensive references, see ref 38.

2.2. Solvation Dynamics

Due to the constant thermal motion of the solute and solvent molecules in the condensed phase environment, the electronic transition frequencies of the solute molecules exploring different solvent environments are not static. Indeed, in the time-correlation function approach mentioned above, the electronic spectral line shape is calculated from the fluctuations in these frequencies. While using the spectral line shape to gain information about the solvent dynamics is possible under certain conditions and has been studied extensively, time-resolved approaches have the potential to give more direct information about the structure and dynamics of the solvent−solute complex, as well as the detailed intermolecular solvent−solute interactions. These approaches have been developed and used since the early 1980s.[17,27,33,41,44,82−85] They are based on the preparation and subsequent probe of an initial solvation state that is far from equilibrium as it evolves toward a new equilibrium state. At the molecular level, these dynamics involve rotation and translation of solvent molecules as influenced by the interactions with the solute molecule in its new electronic state. Theoretical studies are numerous[15,18−26,30,32,34−36,40,42,45,48−50,52,54,56,86−88] and have been extensively reviewed.[36,57,89,90] Thus, we give only a brief background in preparation for the review of this topic in sections 3 and 4 below.

The response of a condensed matter environment to a sudden change in the solute electronic structure can be experimentally detected by various techniques such as time-resolved fluorescence (TRF), transient hole-burning, and photon echo experiments. In many cases, a simple and efficient approach to describing the result uses a (nonequilibrium) time-correlation function defined as

$$S_\omega(t) = \frac{\omega(t) - \omega(\infty)}{\omega(0) - \omega(\infty)} \tag{2.4}$$

where $\omega(t)$ is some time-dependent characteristic frequency (typically taken to be the peak frequency or the average frequency) associated with the line shape. For example, in TRF experiments, $\omega(0)$ is the peak emission frequency immediately after the solute was excited (which is the same as the equilibrium peak absorption spectra for a two-level system). As the solvent responds to the new electronic state, the emission spectrum evolves and $\omega(\infty)$ is the peak of the "final" equilibrium emission spectrum. Equation 2.4 essentially depicts the normalized transient solvatochromic (Stokes) shift[82,83] (see schematic representation in Figure 1).

Computer simulations can easily be used to compute the above nonequilibrium correlation function. Using the simple two-state model mentioned above, we again let H_{gr} and H_{ex} denote the total Hamiltonian of the system when the solute is in the ground and excited electronic states, respectively. Following a sudden transition, the initial ground-state equilibrium distribution evolves under the new excited-state Hamiltonian. The solvent response can be monitored by following the time-dependent energy gap, $U[\mathbf{r}(t)] = H_{ex} -$

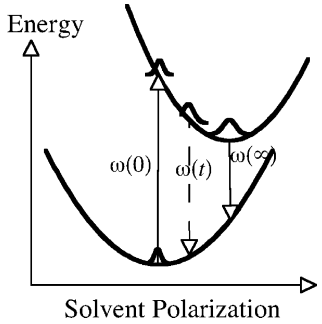

Figure 1. A schematic representation of the energetics involved in a typical time-resolved fluorescence experiment measuring solvation dynamics.

H_{gr}, through the nonequilibrium time-correlation function:

$$S(t) = \frac{\overline{U(t)} - \overline{U(\infty)}}{\overline{U(0)} - \overline{U(\infty)}} \tag{2.5}$$

where $\overline{U(t)}$ is the nonequilibrium ensemble average of $U[\mathbf{r}(t)]$ at time t. Note that $\overline{U(0)} = \langle U \rangle_{gr}$ and $\overline{U(\infty)} = \langle U \rangle_{ex}$ are the equilibrium averages in the initial and final states. In practice, a set of initial conditions selected from the ground-state Boltzmann distribution are propagated under the Hamiltonian H_{ex}, and the energy gap at each time step is recorded and used to compute the averages in eq 2.5. It is clear (within a Franck−Condon approximation) that the $S(t)$ in eq 2.5 is identical to the experimental function in eq 2.4. (For a further discussion of this relation, see ref 22). Note that while the above description is general, many of the published calculations have been for a sudden change in a solute molecule charge or electric dipole moment. For examples involving nonpolar solvents see refs 40, 54, and 91.

Another approach to study the solvation dynamics is based on examining the equilibrium fluctuations in the energy gap $\delta U(t) = U[\mathbf{r}(t)] - \langle U \rangle$. These are used to compute the time-dependent equilibrium correlation function:

$$C(t) = \frac{\langle \delta U(t) \delta U(0) \rangle}{\langle \delta U(0) \delta U(0) \rangle} \tag{2.6}$$

where the ensemble averages are calculated with the Hamiltonian of the excited state. If the time-dependent line shape is approximated by using equilibrium ensemble averages, then one can show that[22,40]

$$S_\omega(t) = S(t) = C(t) \tag{2.7}$$

This is the linear-response approximation. Analytical theories of solvation dynamics are typically based on some approximation to $C(t)$ using equilibrium statistical mechanics or a continuum electrostatic model. In the latter case (which applies to polar solvent dynamics), the frequency-dependent dielectric response $\epsilon(\omega)$ of the medium is required as an input.[36] For example, a very simple model is the Debye model for which $\epsilon(\omega) = \epsilon_\infty + (\epsilon_0 - \epsilon_\infty)/(1 + i\tau_D\omega)$. This model predicts a single-exponential relaxation:

$$C(t) = e^{-t/\tau_L}, \quad \tau_L = \epsilon_\infty \tau_D / \epsilon_0 \tag{2.8}$$

where τ_L is the observed relaxation time (also called the longitudinal relaxation time), τ_D is the Debye relaxation time (a measure of the time it takes for the polarization of a macroscopic sample of liquid to decay to zero after the electric field has been turned off), and ϵ_0 and ϵ_∞ are the static and infinite-frequency dielectric constants of the liquid. While this model gives the correct order of magnitude result, it is not very accurate, and it can be improved by selecting more sophisticated models of $\epsilon(\omega)$ (for example, as a sum of Debye-like terms for different molecular motions[82]) and considering the finite size and mass of the liquid molecules.[20,92−94] Here we summarize the main findings of the experimental and theoretical studies, which are relevant for a comparison with the interfacial systems. For more details about specific systems, the reader should examine the references listed at the top of this section.

1. The nonequilibrium correlation functions are typically not a single exponential. They include an early very fast (less than 50 fs[33]) inertial component, which can account for 60%−80% of the total relaxation in water. This is followed by a multiexponential relaxation on the hundred femtosecond and picosecond time scales.[95]

2. Molecular details of the solvent are important, and in many cases, the relaxation time can be associated with specific molecular motions such as hydrogen bonding dynamics and the rotation of solvent molecules or particular functional groups.[45,82]

3. Simulations show that most of the contribution to polar solvation dynamics comes from the first solvation shell.[25] However, a simple decomposition to uncorrelated distance-dependent contributions is not possible, at least for the models studied.[88]

4. Solute dynamics (rotation and translation) can accelerate solvation dynamics, depending on the relative rate of solvent and solute motions.[96]

5. With few exceptions,[24,34,97] polar solvent dynamics are in reasonable agreement with linear-response theory, even for large perturbations away from equilibrium. Cases where linear response theory fails involve situations where the equilibrium fluctuations do not sample all the regions in which the nonequilibrium dynamics take place.[56]

6. Solvation dynamics in liquid mixtures are sensitive to the mixtures' composition and may reflect clustering and enrichment of one of the solvents around the solute.[34,41,50,98−100]

2.3. The Structure and Dynamics of the Neat Interface

Clearly, knowledge about the molecular structure and dynamics of the neat interface is a prerequisite for a discussion of electronic transitions of solute molecules adsorbed at the interface. Several reviews of the current knowledge about the structure and dynamics of the neat interface have been published during the last 7−10 years.[101−104] In this section, we summarize the main points and in several places update these reviews with more recent results. Most of our current understanding has been obtained from improvements to spectroscopic[105,106] and electrochemical methods[107,108] and from relatively new experimental tools, such as nonlinear spectroscopy,[58,102,109−114] light scattering,[115,116] neutron diffraction,[117−120] X-ray scattering,[121−128] and fluorescence anisotropy decay,[129,130] and theoretically from molecular dynamics and Monte Carlo simulations[101,104,131] and approximate statistical mechanical theories,[132−135] such as density functional theory.[135,136]

Liquid interfaces may be characterized macroscopically by the surface tension and by several nonuniform thermo-

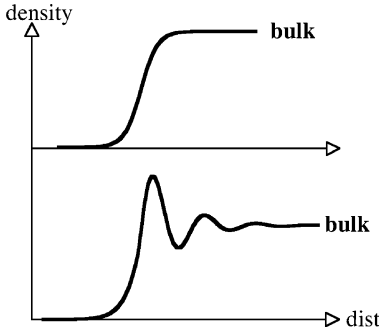

Figure 2. Two typical density profiles of liquid at interfaces. The top profile is observed at most liquid/vapor interfaces and the bottom profile at some liquid/liquid and most liquid/solid interfaces.

dynamic properties, such as density, viscosity, and dielectric response,[105,132,133,137] and molecularly by various single particle and pair correlation functions.

2.3.1. Average Density and Density Fluctuations at Liquid Interfaces

The most extensive knowledge about liquids at interfaces is available on the density variations at the interface. We consider a situation where, due to gravity and far from the critical point, a stable planar interface exists between a liquid and another phase (a different immiscible liquid, a vapor, or a solid). We take z to be the direction normal to the interface. Due to symmetry, an ensemble average of the local atomic density $\rho(x,y,z)$ gives rise to a density profile $\rho(z) = \langle\rho(x,y,z)\rangle$. The plane $z = Z_G$, called the Gibbs dividing surface, can always be selected such that the excess density of the liquid (or one of the liquids in the case of a liquid/liquid interface) on one side can be exactly balanced by the decrease in density on the other side.[133,138] This is approximately where the density is 50% of the bulk value for the liquid/vapor and liquid/liquid interfaces. In what follows, we use the term "surface region" for the region centered at the Gibbs surface, where behavior different from the bulk is observed.

The density profile and density fluctuations along the normal to the interface have been the subject of numerous theoretical treatments, including mean field theories,[133] integral equations, and classical density functional theory,[135,136] and mostly molecular dynamics and Monte Carlo computer simulations.[101−104] Experimentally, the density profile can be determined directly by light scattering techniques[115,116] and by X-ray and neutron scattering.[127]

Two distinct types of density profiles have been observed (or computed), and they are illustrated in Figure 2. In one type, the density profile changes monotonically from the value of one bulk phase to the value of the other bulk phase. In the second type, dampened oscillations exist in the interface region, corresponding to molecular layers packed at the interface. The monotonic density profile has been observed in computer simulations for most liquids at equilibrium with their vapors far below the critical point[101] and in some liquid/liquid interfaces.[139,140] Oscillations are observed in the liquid/vapor interface of liquid metals[141−144] in some simulations[145−150] and density function theories of liquid/liquid interfaces,[136] and are typical for liquids adsorbed on solid surfaces.[135,138]

A monotonic density profile is also the result of capillary wave and van der Waals mean field theories.[133,134,151] In particular, capillary wave theory views the interface as having an intrinsic profile with a finite width, on top of which are superimposed thermally excited capillary waves. By assigning to each wave vector a free energy functional that includes surface deformation (proportional to the surface tension γ) and the contribution due to earth's gravity (g) and summing up all wave vectors (with a proper Boltzmann weighting) from the lower limit of $2\pi/L$ (where L is the size of the square surface area) to the upper limit of $2\pi/\xi_b$ (where ξ_b is the liquid bulk correlation length − a few molecular diameters), one obtains[133,151,153]

$$\rho(z) = \frac{1}{2}(\rho_A + \rho_B) - \frac{1}{2}(\rho_A - \rho_B)\,\mathrm{erf}\left(\frac{z - Z_G}{\sqrt{2}\sigma}\right) \quad (2.9)$$

where erf is the standard error function, Z_G is the average location of the interface, ρ_A and ρ_B are the densities of the two bulk phases, and σ is the interface width, calculated as the mean-squared deviation of the local surface deformation and given by

$$\sigma^2 = (4\pi\beta\gamma)^{-1} \ln \frac{1 + (2\pi l_c/\xi_b)^2}{1 + (2\pi l_c/L)^2} \quad (2.10)$$

where $l_c = [\gamma/\{g(\rho_A - \rho_B)\}]^{1/2}$ is called the capillary length (a few millimeters for water at room temperature). Note that in the thermodynamic limit ($L \rightarrow \infty$) the interface width exhibits logarithmic divergence as $g \rightarrow 0$, so gravity is necessary to establish a stable interface. However, for a microscopic size sample (like the one used in molecular dynamics or Monte Carlo simulations), $\sigma^2 = (2\pi\beta\gamma)^{-1} \ln L/\xi_b$ and gravity does not play a role.

Some of the predictions of capillary wave theory have been confirmed in experiments[115,123,154] and simulations.[101,104,155] For example, since the free energy associated with a local surface deformation is quadratic in the local heights, one expects a Gaussian distribution of local interface positions.[156−158] This has been examined in detail[139,140,146] and found to hold down to a surface area of ξ_b^2. The logarithmic dependence of the interface width on the surface area (eq 2.10) was demonstrated by Senapati and Berkowitz.[155] Recently, Schlossman and co-workers have used X-ray reflectivity to demonstrate that for water/*n*-alkane interfaces, deviations from capillary wave theory can be explained by adding to the capillary wave width (eq 2.10) a contribution from the intrinsic structure of the liquid molecules.[126,154]

The shape of the density profile of several liquid/liquid interfaces (especially that of water) obtained from simulations is also monotonic and can be fit to capillary wave theory using a surface tension γ calculated from independent simulations.[104] However, there is evidence from molecular dynamics simulations[145−150] and density functional theory calculations[136] for dampened oscillations in the densities on the bulk side of the liquid/liquid interfacial region, as shown in Figure 2. While the oscillatory density profile of liquids near solids observed in simulations,[159−169] statistical mechanical theories,[135,170,171] and experiments[172−175] reflects the layering of molecules packed on relatively fixed solid atoms, it is not clear that a similar phenomenon is at play in the liquid/liquid system. For example, Toxvaerd and Stecki found stable equilibrium oscillatory structures in the density profiles of two immiscible Lennard-Jones liquids, but these vanish with the increase in the surface area.[147] In liquid/solid systems, the decay length of the oscillations depends on the type of intermolecular forces and the size of the liquid molecules.

For water next to a variety of surfaces, the bulk density is reached in three to four molecular layers (10−12 Å).

The average density at the liquid interface (which is reflected by the density profile) is expected to play a role in some aspects of solvation dynamics, as will be shown later. More generally, the dynamics of solvent and solute molecules in the interfacial region are affected by the effective viscosity of the medium, and this is directly related to the density. This will be discussed further below.

While the density profile and, by association, the average local density are concepts of fundamental importance, their effects are typically well understood by proper extrapolation from the behavior of bulk homogeneous systems as a function of density. More unique to the interface region are the density fluctuations that give rise to the finite interface width. Although the description of these density fluctuations in terms of thermally excited capillary waves is a reasonable approach (which enables one to make a connection with the macroscopic surface tension), only the lower wavelength limit (near ξ_b) could be coupled to molecular motions. Thus, it is the local surface deformation that is more relevant to an understanding of the behavior of solutes at interfaces.

Most of the evidence for the coupling of local surface roughness to molecular motion comes from molecular dynamics simulations. For example, in ion transfer across the interface between two immiscible liquids, fingerlike structures of water molecules can form and either inhibit or enhance ion transfer, depending on the driving force of the transfer.[176−182] In electron transfer, surface roughness may enable the reactants to approach each other with a larger angle, thus increasing the effective reaction volume.[183] We will see later that dynamic surface roughness is also important in understanding electronic spectra and solvation dynamics at interfaces.

Demonstrating this surface roughness experimentally is more challenging. Using fluorescence depolarization experiments, Wirth and co-workers have shown that the reorientation dynamics and the lateral diffusion of acridine orange dye at several water/hydrocarbon interfaces do not correlate with the bulk viscosity of the bulk media or with the surface tension,[129,130] but are affected by the molecular shape of the solute and the roughness of the interface. Molecular shape considerations maybe also be important in electronic spectra at the interface, as will be discussed later. Somewhat more direct information about the local roughness of liquid surfaces can be obtained by the scattering of atoms and molecules from the free liquid surface.[184−186] For example, the orientational distribution of the scattered atoms and molecules and their energy distributions can be related to local surface corrugation.[184,187−189]

2.3.2. Molecular Structure and Dynamics

Molecules at the interfacial region are subject to strong asymmetry in the intermolecular forces, which may result in a molecular structure and dynamics at the interface significantly different from those in the bulk. Some of the most dramatic advances in the knowledge about liquids at interfaces have been concerning their molecular structure, and while most of this knowledge has been obtained from molecular dynamics and Monte Carlo simulations, there is a growing number of experimental studies, as will be briefly discussed below.

2.3.2.1. Molecular Orientation For a system of N particles whose mutual interactions can be described classically by a potential energy function $U(\mathbf{r}_1, ..., \mathbf{r}_N)$ where $\mathbf{r}_1$, ..., $\mathbf{r}_N$ are the positions of all the particles, the singlet distribution function defined as $\rho^{(1)} = N\int \exp(-\beta U)\, d\mathbf{r}_2 ... d\mathbf{r}_N / \int \exp(-\beta U)\, d\mathbf{r}_1\, d\mathbf{r}_2 ... d\mathbf{r}_N$ is constant for a homogeneous system and equal to the bulk density N/V. The cylindrical symmetry at a planar interface gives rise to a $\rho^{(1)}$ that is a function of z, the density profile. If the liquid is molecular, the z-dependence of the singlet distribution suggests that at the interface there is a nonrandom orientational preference, which can be described using an orientation profile: $P(z,\theta)$ is the probability density that a molecule whose center of mass is at z will have the angle θ between a vector fixed in the molecule frame of reference and the normal to the interface. Knowledge of molecular orientations is important for understanding equilibrium solvation structure of adsorbed species and thus their electronic absorption spectra.

Theoretical studies until 1996 have been reviewed in ref 60, and since then a number of molecular dynamics and Monte Carlo studies have been published.[150,190−193] Most of the recent experimental data on molecular orientations at liquid surfaces have been obtained using nonlinear second harmonic generation (SHG) and sum frequency generation (SFG) spectroscopies.[111,194−200]

Several general observations can be made regarding orientational preference at liquid/vapor and liquid/liquid interfaces:

1. Molecular dynamics and Monte Carlo simulations show that most orientational distribution functions are quite broad, reflecting a free energy difference between the most likely and least likely orientation to be on the order of a few kT. This is consistent with experimental data.[201]

2. Water molecule orientation at hydrophobic surfaces reflects the tendency to maximize hydrogen bonding, and this gives rise to orientations where the water dipole typically lies parallel to the interface with one OH bond pointing toward bulk water. This seems to be independent of the nature of the water intermolecular potential, but other orientational properties, such as the H−H vector may be more sensitive to the choice of the potential energy function.[103] As pointed out by Jedlovszky,[150] describing water orientation using the distribution of only one angle may be misleading, and water orientation specified by using the joint probability distribution of two independent angles may be useful for elucidating multiple preferred orientations.

3. Some of the clearest data about water orientation at hydrophobic surfaces, about its dependence on external fields and on the nature of the hydrophobic phase, have been obtained in recent years using SFG spectra. Shen and coworkers first demonstrated the existence of dangling OH bonds at the water liquid/vapor interface, which can be quenched by the addition of methanol.[202,203] Detailed studies by Richmond and co-workers extend this work to the interface between water and CCl_4, 1,2-dichloroethane, and liquid alkanes.[112,204−208]

4. The hydrophobic end of a molecule adsorbed at a water surface tends to point away from the aqueous phase. This expected result has been used in recent years as a validation of new experimental techniques for measuring orientations.[200]

5. It is straightforward to demonstrate the dependence of water molecular orientation on external field by molecular dynamics simulations.[165,166,168,209−211] Nonlinear spectroscopy has been used to study water orientation change induced by adsorbed charged molecules,[212−214] and this can have a

marked effect on its hydrogen bonding structure.[112] Of course, much work has been done on water orientation at charged metal electrodes, but this is outside the scope of this review.

2.3.2.2. Pair Correlation. The two-body distribution (or pair correlation) function, defined as $\rho^{(2)}(\mathbf{r}_1,\mathbf{r}_2) = N(N-1)/2 \int \exp(-\beta U)\, d\mathbf{r}_3 \ldots d\mathbf{r}_N / \int \exp(-\beta U)\, d\mathbf{r}_1\, d\mathbf{r}_2 \ldots d\mathbf{r}_N$, is proportional to the probability of finding a particle at the position $\mathbf{r}_1$, given that there is a particle at the position $\mathbf{r}_2$. In bulk homogeneous systems, this is a function of only the interatomic distance $r = |\mathbf{r}_2 - \mathbf{r}_1|$. However, at a planar interface, it is also a function of the locations z_1 and z_2 of the two particles along the interface normal. While this quantity is of fundamental importance in the development of statistical mechanical theories of liquids at interfaces,[133,135] it is cumbersome to compute and impossible to measure. Thus, one is usually interested in an average over z_1 and z_2 within some thin slab centered around z. This gives an orientationally averaged radial distribution function g for different slices along the interface normal: $g(r;z)$. We will refer to this function as simply the interfacial radial distribution function (RDF). The extended X-ray absorption fine structure method (EXAFS), which was recently used to measure nearest neighbor O−O distances for surface water molecules, is an experimental approach to similar types of data.[215]

Interfacial radial distribution functions are very useful for describing the solvation environment of a solute molecule adsorbed at the interface, as will be discussed in sections 3 and 4 below. Here we mention a few characteristics of this function for neat liquids and refer the reader to existing reviews for more details.[60]

One important feature of polar liquids is the tendency to keep the structure of the first coordination shell relatively similar to that in the bulk.[140,216,217] This is reflected in the observation that the peak position of the interfacial RDF is very close to the peak position of the bulk RDF and that the peak height is only slightly reduced. In contrast, the second peak is typically much smaller than that in the bulk, reflecting the reduced average local density at the interface. For an obvious reason, the asymptotic value (as $r \rightarrow \infty$) of the interfacial RDF is near 0.5 instead of 1. The exact variation of the height of the first peak with the distance z along the interface normal depends on the system, but it normally begins to drop well below the bulk value only significantly passed the Gibbs surface. For nonpolar liquids, a significant reduction in the first peak can already be observed near the Gibbs surface, although the peak position is generally unaffected.[140]

2.3.2.3. Hydrogen Bonding Structure and Dynamics. Hydrogen bonding has been the focus of many studies of interfacial water. Most of our current (though incomplete) understanding is derived from SFG spectroscopy, where the vibrational spectra of water at the air/water interface, at the interface with immiscible liquids, and at solid and solidlike surfaces have been measured.[112,204−208,214,218−220] These spectra are broad with features that are assigned to disordered water, icelike strongly hydrogen-bonded water, and, in some cases, "free" OH bonds. By examining the relative contribution of these different features as a function of the other phase and of solute concentration, information about the interfacial structure can be obtained. However, these assignments are still debated.[112] Combined molecular dynamics simulations and experiments are and will continue to be of great help in sorting out the relationship between hydrogen bonding structure and the features in the SFG spectra.[221−224]

In theoretical studies of hydrogen bonding the situation is somewhat clearer, because a working (although quite arbitrary) definition of hydrogen-bonding is possible. One choice is to define two water molecules to be hydrogen-bonded if their mutual interaction energy is more negative than 10 kJ/mol. Other definitions that have been used include an oxygen−oxygen distance being less than some cutoff (typically taken to be the first minimum in the OO radial distribution function, about 3.5 Å),[139,140,225,226] as well as restricting the OHO angle to some value (20°−40°).[227] The exact choice of the structural parameters is not expected to significantly change some of the calculated properties (such as the hydrogen bond's lifetime[227−229]), although the exact number of hydrogen bonds will be affected by the exact choice.

Using the above definition of hydrogen bonding, one finds that on average each water molecule in bulk water is hydrogen bonded to 3.6 other water molecules. At the interface (liquid/vapor and liquid/liquid with polar as well as nonpolar liquids), this number drops to 2−3 depending on the exact location along the interface normal. However, when this number is divided by the total number of water neighbors, the ratio is larger at the interface.[139,140,146,148,149] This was interpreted[153] as suggesting that the hydrogen bond lifetime is longer at the interface. The calculated hydrogen-bond lifetime using the time-correlation function method is generally in agreement with this at water/solid[230−232] and water/liquid interfaces,[233] as well as at liquid/vapor interfaces, if the contribution due to diffusion is taken into account.[234]

Understanding the hydrogen bond structure and dynamics at interfaces is very much still an open problem. Recent developments of broadband sum frequency generation spectroscopy[235] and its application to liquid surfaces[236] suggest that new contributions are expected soon, especially in the experimental study of hydrogen bond dynamics.

2.3.2.4. Dynamics. The anisotropy in surface forces is also reflected in the dynamics of molecular motion such as rotational dynamics and molecular diffusion. Most of the experimental data available concerns solute rotational dynamics, so again most of the direct knowledge about pure solvent molecule dynamics accumulated in recent years is from molecular dynamics simulations. Since understanding solvent molecule dynamics is fundamental to elucidating solvation dynamics, we consider this subject here in some details.

Concerning first the diffusion of solvent molecules at the interface, instead of the scalar diffusion coefficient in bulk liquid, one must deal in a general inhomogeneous environment with a diffusion tensor. The cylindrical symmetry at planar liquid/vapor or liquid/liquid interfaces gives rise to two independent elements of the diffusion tensor: $D_\perp(z)$ and $D_\parallel(z)$ are the elements normal and perpendicular to the interface, respectively, both of which depend on the location relative to the interface and both of which should approach the bulk value as z approaches a location far from the interface. Care must be taken in computing the anisotropic diffusion coefficients by the standard mean square displacement method used in the bulk, since the diffusing molecules parallel to the interface may change their location during the simulation, and the motion perpendicular to the interface is influenced by an effective potential of mean force.[237] Published simulation results give in general the result $D_\perp(z)$

$< D_{\parallel}(z)$ at liquid/vapor[237] and liquid/liquid[140,149] interfaces. However, while the above calculations give $D_{\perp}(z) < D$(bulk), the recent analysis of Berne and co-workers suggest that at the liquid/vapor interface, both the normal and the perpendicular component of the diffusion tensor are larger than the bulk diffusion constant.[237] At the liquid/solid interface, there are experimental data supporting a higher viscosity of the liquid film adsorbed on the solid surface.[238,239] Computer simulations are consistent with a slowing of solvent diffusion but suggest that the solid influence is limited to a nanometer-thick solvent region.[169,211,240]

Rotational dynamics are typically described using orientational correlation functions.[241,242] If $\hat{e}_r$ is a unit vector along a molecule-fixed vector, then a measure of the reorientation dynamics around this axis is provided by the set of time-correlation functions:

$$C_l(t) = \langle P_l[\hat{e}_r(t+\tau)\cdot\hat{e}_r(\tau)]\rangle \qquad (2.11)$$

where the angular brackets represent an ensemble average over all solvent molecules in the interface region (or in the bulk) and over all time origins τ such that τ is less than the residence time of the molecule in the given region. $P_l(x)$ is the l-th order Legendre polynomial. In the bulk phase, this function decays exponentially and may have some oscillatory structure, depending on the density and the temperature.[17,241,242]

Molecular dynamics simulations show that for water the dipole reorientation time (which may be related to IR spectral line shape) is only mildly different at the interface[140,164,243] from the value in the bulk[244] (around 2 ps). Similarly, the H−H vector reorientation time (which determines the NMR line shape) is only slightly affected. For example, the reorientation dynamics at the liquid/vapor interface are slightly faster than those in the bulk, probably due to the reduced friction (as a result of the reduced density), whereas at the water/DCE interface it is slightly slower than in the bulk.[140] In contrast, much slower dynamics are observed for the first layer of water at the solid/water interface[169,211,240] and for water in the pool of reverse micelles.[245,246] These numbers seem to reflect the strength of the interaction between water and molecules of the other phase. External electric fields, which break down the hydrogen bond network, give rise to moderate acceleration in the molecular rotation and diffusion time.[103,210]

An interesting dynamical behavior that is unique to the interfacial region is the dynamic associated with surface deformations at length scales from just above the bulk correlation length to macroscopic (hydrodynamics). Those on the shorter end of this length scale may be relevant to the behavior of a solute molecule, as will be discussed below. These surface deformations have been characterized at the water/DCE interface.[140] They can be thought of as transverse density fluctuations ("fingers"), whose dynamics are on the tens of picoseconds time scale.

2.3.3. Polarity and Dielectric Behavior

One of the most important properties of the liquid interface region that is a significant focus of this review is the degree to which ionic and polar species adsorbed at the interface can be solvated. While the static dielectric constant ϵ (and more generally the frequency-dependent complex dielectric function $\epsilon(\omega)$) of the bulk liquid is an important ingredient in this regard, it is not clear how to generalize this to the inhomogeneous region. More important is the realization that the solvent−solute interactions that are responsible for the stabilization (or destabilization) of ionic and polar solute molecules relative to the bulk may be quite complex and cannot in general be represented by one quantity.

We will discuss the effective polarity scale of the interface in section 3. Here we make a few comments regarding the dielectric response of a liquid at the interface. In general, this quantity reflects all of the interfacial structural and dynamic characteristics discussed above.

While the dielectric response of pure liquids, and of water in particular, has been the subject of intense experimental and theoretical studies,[57,247,248] not much is known about the dielectric behavior of pure interfacial water. This reflects the difficulties of a direct experimental probe of the buried interface and of applying the statistical mechanical theory of the dielectric response to the inhomogeneous region. A very simple concept, which has been used in simple continuum models of interfaces to calculate adsorption free energy and electronic spectra, is that of an effective interfacial dielectric constant. In general, the reduced orientational freedom (such as that observed at the water/solid interface) and the reduced density (as in the liquid/vapor interface) result in a smaller effective dielectric constant than that in the bulk, and experiments that will be discussed later are generally in agreement with this picture. For example, a dielectric constant of 5−10 for the few water layers adsorbed on the metal electrode is used to explain capacity measurements and the spectroscopic line shape shifts of adsorbed species.[10]

Another simple approach that has been extensively used[137,249,250] is to assume that the dielectric constant is equal to the bulk value up to a mathematically sharp interface, where it jumps to the constant bulk value of the second phase. A solution of the electrostatic boundary problem can be represented in terms of image charges, and the interface effect is described as the result of interactions between the solute molecules and these image charges. Most continuum electrostatic treatments of the interface use this model and its application to electronic spectra will be described in section 3.2. It is important to note that this description becomes increasingly inaccurate as one approaches distances from the interface that are comparable to the size of a solute molecule.

3. Electronic Spectroscopy at Liquid Interfaces

3.1. Experimental Data

3.1.1. Nonlinear Optical Studies of Liquid/Vapor and Liquid/Liquid Interfaces

While linear spectroscopic techniques such as UV−vis absorption spectroscopy (used to obtained bulk electronic spectra) can be used to study some interfacial systems (thin films, adsorbed monolayers, and micelles and microemulsions), nonlinear spectroscopy techniques are the appropriate methods for measuring electronic spectra of solute at interfaces when there is also a substantial amount of the solute in the bulk region. The surface selectivity of SHG and SFG make it possible to obtain the signal from the surface molecules unmasked by a contribution from the bulk, since second-order nonlinear optical processes are dipole-forbidden in centrosymmetric media.

Resonant SHG is a method that is sensitive to the magnitude and orientation of electronic transition moments,

and thus it is ideal for studying electronic spectra of adsorbed species. In a typical experiment, a single laser beam of frequency ω is focused on the interface, and the intensity of a nonlinear polarization with frequency 2ω is detected. This intensity is given by[58]

$$I(2\omega) = (32\pi^3\omega^2/c^3)\sec^2\theta\,|\hat{e}(2\omega)\cdot\vec{\vec{\chi}}^{(2)}:\hat{e}(\omega)\hat{e}(\omega)|^2 I^2(\omega) \tag{3.1}$$

where c is the velocity of light, θ is the angle between the incident laser beam and the normal to the interface, ω is the frequency of the incident beam with the unit polarization vector $\hat{e}(\omega)$ and intensity $I(\omega)$, and $\hat{e}(2\omega)$ is the unit polarization vector of the detected beam. $\chi^{(2)}$ is the second-order susceptibility of the medium, which is a third-rank tensor (27 elements) that can be written as a sum of a nonresonant $\chi^{(2)}_{NR}$ and a (much larger) resonant term given by the molecular hyperpolarizability (ignoring solute−solute interactions):

$$\chi^{(2)}_R = N_s\sum_{v,e}\frac{\langle g|\mathbf{r}|v\rangle\langle v|\mathbf{r}|e\rangle\langle e|\mathbf{r}|g\rangle}{(\omega - \omega_{gv} + i\Gamma_{gv})(2\omega - \omega_{eg} - i\Gamma_{eg})} \tag{3.2}$$

where N_s is the surface density of molecules, $|g\rangle$ is the ground state, $|e\rangle$ is any excited state that contributes to the signal and $|v\rangle$ is an intermediate virtual state. ω_{ij} and Γ_{ij} are the frequency and dephasing rates of the $|i\rangle \rightarrow |j\rangle$ transition, respectively. Clearly, a resonant enhancement occurs when either $\hbar\omega$ or $2\hbar\omega$ approach the ground to excited-state energy difference, $\hbar\omega_{eg}$, thus enabling the measurement of an effective electronic excitation spectrum. Note that the peak of the *observed* SHG spectrum does not necessarily match ω_{eg}, due to the contribution of the nonresonant term, which, however, can be removed by a fitting procedure.[251] In addition to the requirement that the system be noncentrosymmetric, the detection of the SHG signal also requires that the solute molecules have appreciable hyperpolarizability. Furthermore, because of the buried nature of the liquid/liquid interface, to prevent absorption of the signal in one of the bulk phases one typically uses the total internal reflection geometry,[252−255] in which the incident beam approaches the interface at an angle to the surface normal that is greater than the critical angle, $\theta_c = \sin^{-1}(n_1/n_2)$, where n_1 and n_2 are the refraction indices on the two bulk phases. While the present review is limited to electronic spectroscopy, the review articles listed in the first paragraph of section 2.3 discuss at length the application of SHG to many other measurements, such as surface concentration, orientation, relaxation, and chemical reaction dynamics.

The first demonstration of using SHG to determine solvatochromic shift at liquid interfaces was by Wang, Borguet, and Eisenthal, who measured the SHG spectrum of the intramolecular $\pi \rightarrow \pi^*$ charge-transfer band of the polarity indicator molecule *N*,*N*′-diethyl-*p*-nitroaniline (DEPNA) at the air/water interface.[251] The DEPNA charge-transfer band, which is centered at 329 nm in the gas phase,[256] is red-shifted to 429 nm in bulk water[251] but to only 359 nm in bulk hexane (nonpolar solvent).[80] At the air/water interface, the charge-transfer peak is at the intermediate value of 373 nm, which is very similar to the peak position in bulk carbon tetrachloride (375 nm) and butyl ether (372 nm).[80] This indicates that the water/air interface has a polarity similar to that of these two liquids (at least as it concerns the interaction with DEPNA). The positive solvatochromic shift

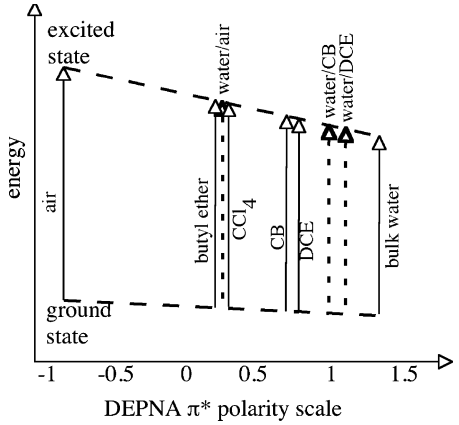

Figure 3. A schematic representation of the measured polarity of several bulk liquids and liquid/liquid interfaces using DEPNA (*N*,*N*′-diethyl-*p*-nitroaniline) as the solvatochromic probe. The solid arrows represent the transition energy in the bulk liquids and the dashed arrows at the interfaces. Adapted from ref 257.

of DEPNA is mainly due to the large increase in the electric dipole moment upon excitation (from 5.1 to 12.9 D). As pointed out by Eisenthal and co-workers, the above result is general in the sense that a similar polarity of the air/water interface was obtained[257] using the $E_T(30)$ polarity indicator (which exhibits negative solvatochromism).

The above approach was extended by Eisenthal and co-workers to the liquid/liquid interface by studying the SHG spectra of DEPNA adsorbed at the water/1,2-dichloroethane and water/chlorobenze interface.[257] The resulting polarity of these interfaces, as well as the air/water interface and several bulk liquids, is given in Figure 3. The polarity can be conveniently expressed using the normalized scale[81]

$$\pi^* = \frac{\omega_{max}(\mathrm{cm}^{-1}) - 27\,520}{-3182} \tag{3.3}$$

An interesting point noted by Eisenthal is that the polarity of each of the three interfaces (indicated by the vertical dashed line) is very close to the arithmetic average of the polarities of the two bulk phases. A similar result was obtained using the $E_T(30)$ indicator for the water/air and the water/heptane interfaces,[257] suggesting that this could be a general result. Computer simulations[59,258] and simple statistical mechanical arguments[259] suggest that the major contribution to the solvation energy comes from the first solvent−solute coordination shell. Thus, the simple arithmetic rule indicates that DEPNA and the $E_T(30)$ indicator molecules have a mixed solvation environment. Molecular dynamics simulations, which will be discussed later, reproduce some of these data and give additional insight into why the two liquids contribute almost equally to the observed shift.[260,261]

Girault and co-workers measured the resonant SHG spectrum of a doubly charged eosin B at the air/water interface and found that the maximum of the resonance is observed at 533 nm.[262] This is compared with the UV−vis spectrum in bulk water, which has a maximum at 520 nm. Since the spectrum in the gas phase is not available, the arithmetic rule cannot be checked here. However, the spectrum in bulk 1,2-dichloroethane has a maximum at 555 nm, which suggests that the air/water interface is more polar than bulk 1,2-dichloroethane, in contrast with the results of Wang et al.[257] Clearly, despite the loss of stabilization at the air/water interface compared with the bulk and despite

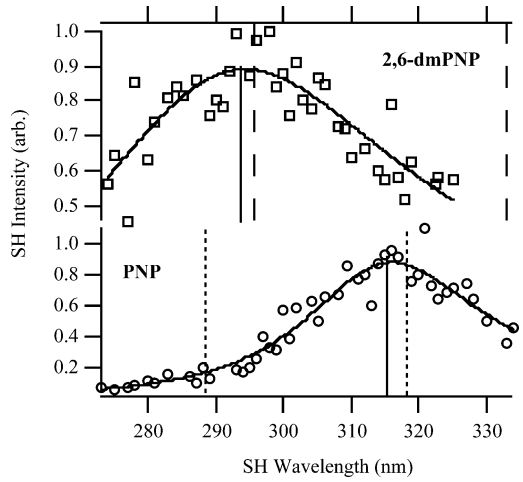

Figure 4. Second harmonic spectra of dmPNP (□) and PNP (○) at the water/cyclohexane interface. The solid lines through the data points are fits to eqs 3.1 and 3.2 (including a nonresonant term), which lead to band positions of 293 and 315 nm, respectively (represented by the vertical solid lines). Dashed vertical lines represent the excitation maxima of dmPNP in bulk cyclohexane (296 nm) and bulk water (334 nm). Dotted vertical lines represent the excitation maxima of PNP in bulk cyclohexane (288 nm) and bulk water (318 nm). Reproduced from ref 263.

the fact that this molecule is not surface-active, the strong field due to the two charges enables the molecule to form enough hydrogen bonds to form a local hydration shell that is more favorable than that in the bulk of a non-hydrogen-bonding liquid. Another way to state this is that while the DEPNA polarity indicator suggests that the air/water interface is less polar than bulk 1,2-dichloroethane, the eosin B result suggests that the air/water interface has a higher hydrogen bond ability index (the Kamlet−Taft α parameter[72]) than bulk 1,2-dichloroethane.

Another example of the observation that properties of the interface depend on more than simply the properties of the two bulk phases has been provided recently by Steel and Walker[263] who used two different solvatochromic probe molecules, *para*-nitrophenol (PNP) and 2,6-dimethyl-*para*-nitrophenol (dmPNP), to study the polarity of the water−cyclohexane interface. Despite the fact that dmPNP is much less polar than PNP, these two probe molecules give spectral shifts as a function of bulk solvent polarity that are very similar, and thus polarity values obtained by one probe are highly correlated with the values obtained by the second probe. This is because both solutes are mainly sensitive to the nonspecific solvent dipolar interactions. And yet, when these two dye molecules are adsorbed at the interface, they experience quite different polarities (Figure 4): The more polar solute (PNP) has a maximum SHG peak at 315 nm, very close to that of bulk water, and thus it reports a high polarity environment. In contrast, the less polar solute (dmPNP) reports a much lower interface polarity; it has a maximum SHG peak at 293 nm, very close to that of bulk cyclohexane. While these results intuitively make sense, this is the first "clean" and direct demonstration that small changes in solute structure can have a major effect on the local solvation environment at a liquid/liquid interface.

An interesting example for similar effects at the air/water interface was presented by Tamburello-Luca et al., who measured the resonant-enhanced SHG of PNP, phenol, and *para*-propylphenol at the air/water interface.[264] Of these, only PNP and phenol had a significant solvatochromic shift. For PNP, the maximum of the SH resonance (310 nm) lies much closer to that in bulk water (322 nm) than to that in bulk hexane (284 nm), indicating that it is nearly fully hydrated. For phenol, the peak spectrum at the air−water interface (267 nm) is much closer to that in bulk hexane (270 nm) than to that in bulk water (258 nm), indicating that it is sampling a highly nonpolar environment (consistent with molecular dynamics simulations[265]). Thus, these two different probes reported very different polarity of the air/water interface.

As was mentioned at the end of section 2.1, attributing the change in the solvatochromism upon transfer of an indicator molecule from the bulk to the interface to a different polarity of the interface assumes that the electronic structure of the molecule is unchanged upon the change in the environment. Nagatani et al. have recently presented an interesting example for the breakdown of this assumption.[266] They have measured the SHG spectra of the free base and the zinc(II) complex of cationic *meso*-tetrakis(*N*-methyl-4-pyridyl)porphyrins, H_2TMPyP^{4+} and $ZnTMPyP^{4+}$, at the water/1,2-dichloroethane interface and compared them to the UV−vis spectra of these two species in the bulk of the two liquids. Although the molecular hyperpolarizability of the symmetrically substituted porphyrins is very small,[267] the adsorbed species give rise to intense SH signals, suggesting that the electronic structure of molecules adsorbed at the interface is modified from the bulk structure. In addition, while the surface SH spectrum of H_2TMPyP^{4+} is similar in shape to the electronic absorption spectrum in bulk water, with a peak location between the peak location in the two bulk phases, the surface SH spectrum of the zinc(II) complex system shows two peaks, one with a maximum intensity at 436 nm coinciding with the bulk aqueous species and a second at 452 nm that is attributed to aggregation of ZnTMPyP monomers adsorbed at the interface.

Resonant SHG spectra have been used previously by others to study association and aggregation at the liquid/vapor interface. Levinger and co-workers found that the resonant SHG spectrum of the laser dye IR125 at the air/water interface is markedly different from the bulk solution spectrum.[268] They attributed this to aggregation driven by surface orientation that is different in nature than the one observed in the bulk at higher concentration or due to added salt. Teramae and co-workers studied the association of rhodamine dyes adsorbed at the heptane/water and hydrophobized silica/water interfaces.[269] The SHG spectra were used to distinguish between different structural arrangements at the two interfaces and as a function of coverage by including polarization measurements. Using resonant SHG spectra, Owrutsky and co-workers demonstrated that several oxazine dye molecules (oxazine 720, cresyl violet, and Nile blue), which are known to form dimers in aqueous solutions, are adsorbed at the interface almost exclusively as dimers.[270] An increase in the bulk solution ionic strength increases the dimer concentration at the surface to a greater extent than that for the bulk solution. While no polarity estimates were given, this result is clearly consistent with the less polar nature of the air/water interface relative to bulk water.

Because the SHG signal is obtained from the entire noncentrosymmetric region, the above experiments are not able to give information about the spatial dependence of the signal across the interface. Continuum electrostatic models and simulations, to be discussed below, show, however, that due to finite interface width the spectra should depend on the location of the probe molecule along the interface normal.

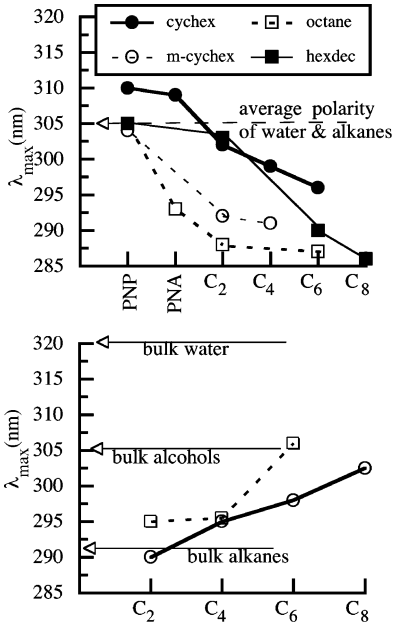

Figure 5. Fitted interfacial SHG maxima for different chromophores adsorbed at different liquid/liquid interfaces. The top panel shows the results for the interface between water and four different alkanes (reproduced from ref 273). The bottom panel depicts the average peak spectra at the interface between water and the linear alchohols 1-octanol and 1-decanol (○) and the branched alcohols 3-octanol and 2,6-dimethyl-4-heptanol (reproduced from ref 274). The arrows denote the absorption maxima in different bulk liquids, as indicated.

To study this experimentally, Steel and Walker have designed a series of solvatochromic probes they call "molecular rulers".[271] Each of these surfactant molecules consists of an anionic sulfate group attached to a hydrophobic solvatochromic probe molecule by a variable length alkyl spacer. The probe molecule is based on *para*-nitroanisole (PNA), whose bulk solution excitation maximum monotonically shifts with solvent polarity from 293 nm in cyclohexane to 316 nm in water.[74] Since PNA is 20 times more soluble in cyclohexane than in water, while the sulfate headgroup is restricted to the aqueous phase, the surfactant molecules will adsorb at the interface with the anionic end in the aqueous phase and the probe molecule at variable positions relative to the interface, depending on the length of the alkyl spacer. The SHG spectra of these surfactants were measured at different water/organic liquid interfaces.[272−274] The maximum of the absorption band as a function of the length of the alkyl spacer at several water/liquid interfaces is shown in Figure 5.

The top panel shows the results for water/alkane interfaces,[272 273] where, in addition to the absorption peaks of the "molecular rulers", results are shown for the "bare" chromophore (PNA) and the more polar probe PNP. When any of these probes is in bulk water, the peak maximum is near 320 nm, and when it is in the bulk alkanes, the peak maximum is between 287 and 295 nm. So we take 291 nm as an average value for bulk alkanes. The average polarity of bulk water and bulk alkanes will then correspond to $\bar{\lambda}_{max} \approx 305$ nm. Walker and co-workers found that in general, as the probe varies from PNA to PNP to C_n, $n = 2$, 4, 6, or 8, the polarity "reported" by the probe varies from the "average" polarity $\bar{\lambda}_{max}$ to that of bulk alkane. This provides direct evidence that the interface is sharp; the width is no greater than the size of a C_6 "ruler", about 1 nm. Interesting variations among the four different liquids suggest a correlation between the width of the interface and the molecular shape and packing at the interface.[273] The SHG spectral width was also found to correlate with the interface width.

The bottom panel of Figure 5 shows very different behavior at the interface between water and a number of long-chain alcohols.[272,274] The polarity of these strongly associating interfaces, as "reported" by the short "rulers", was close to that of bulk alkanes, approaching the bulk alcohols limit when the longest ruler was used. The existence of a very low polarity region at the interface suggests close packing of the alcohol molecules such that their alkane groups give rise to a low polarity region, which is consistent with X-ray scattering experiments.[275] Calculations of the local electric field across the interface via molecular dynamics simulations also confirm the existence of a local low polarity region at the interface.[276] These simulations suggest that only those octanol molecules that are hydrogen bonded to water molecules are aligned perpendicular to the interface. As in the case of the water/alkane interface, the interface width is about 1 nm and is dependent on the molecular shape; it is narrower for the branched alchohols.

Recently, these studies have been extended by Walker and co-workers to include surfactants with cationic headgroups, as well as the effect of electrolytes dissolved in the aqueous phase.[277,278] These experiments underscore the effect of surface charges on the electronic structure of the adsorbed chromophore and on the properties of the adjacent medium.

The experiments described in this section demonstrate that resonant SHG is a powerful and sensitive technique to study the structure of the neat interface by a solute probe. However, one needs to consider three effects that may influence the interpretation of the results: (1) the solute may perturb the interface, (2) the solute electronic structure may be different than that in the bulk, and (3) different solute molecules may be sensitive to different surface characteristics or sample different regions of the interface. Clearly, this area is still developing and considerable work remains to be done, both with the development of the technique and with the interpretations.

3.1.2. Interface Polarity of Micelles and Reversed Micelles

In addition to their intrinsic interest[279,280] (stabilization of chemical species, microenvironment for reaction micelle, and more), reverse micelles and microemulsions offer a convenient way to study the interface between water and an organic (liquid or solidlike) phase. This is because they can be studied with bulk solution techniques, which utilize the large effective surface area of these nanoscale structures.

Many studies have used fluorescent molecules as a probe of the local polarity of the interface. Saroja and Samanta have used the spectral shift of 4-aminophthalimide to determine the effective polarity of the interface between water and micelles formed from cationic (SDS), anionic (CTAB), and neutral (Triton-X) surfactants.[281] In bulk liquids, this probe molecule exhibits a shift of the peak emission spectra of more than 100 nm on changing the solvent from water to 1,4-dioxane. When the probe is adsorbed at the interface, a polarity intermediate to that of water and methanol was found irrespective of the charge of the headgroup. This is in contrast with polarity measurements using pyrenecarboxaldehyde as a probe of the same micelles, which show strong dependence of the polarity on the nature of the micelle headgroup.[282,283] This is apparently due to the

nonpolar nature of the probe molecule, which penetrates deeper into the hydrophobic core and gives rise to lower polarity.[281] This underscores the point that one must take into account the fact that the micelle−water interface may have different absorption sites, so the establishment of a polarity scale for micelles is more problematic than that for a planar liquid/liquid interface.

A study of the interface polarity of AOT (aerosol OT, bis-(2-ethylhexyl)sodium sulfosuccinate) reversed micelles was reported by Laia and Costa,[284] using the solvatochromism of two squaraine dyes. By comparing the observed shift (for emission and absorption) with the shifts in pure water, dioxane, and dioxane−water mixtures, they were able to find good empirical correlations with the π^* polarity scale and the solvent proticity scale (a measure of the solvent acidity character). However, as in the above case, some deviations are observed at low water contents of the reverse micelles, due to the probe distribution at two different interfacial sites.

The complex environment at the micelle−water interface suggests that it is more appropriate to use a multiparameter approach to the description of the solvent polarity. This was done by Vitah et al.[285,286] for the dodecyltrimethylammonium bromide (DTAB) and sodium dodecyl sulfate (SDS) micelles. DTAB micelles were found to be quite polar ($\pi^* = 1.02$), to have relatively strong hydrogen-bond donating ability ($\alpha = 0.700$), and to have moderate hydrogen bond accepting ability ($\beta = 0.486$), which is very similar to SDS micelles ($\pi^* = 1.06$, $\alpha = 0.87$, $\beta = 0.40$). A comparison with solvatochromic parameters of some pure solvents such as DMSO ($\pi^* = 1.00$), 2-propanol ($\alpha = 0.69$), and ethylbenzoate ($\beta = 0.43$) suggests that the micellar environments observed by the various indicators are quite dipolar with very strong hydrogen bond donors and moderately strong hydrogen bond acceptors. Both the high polarity and the strong hydrogen bond acidity support previous work, which indicates that water is present in the indicators' micellar microenvironments.

An important class of reverse micelles, which has interesting practical applications and is also of fundamental interest is made from a nonaqueous polar solvent (and a nonpolar solvent). Levinger and co-workers[287] have used the absorption spectra of coumarin 343 dye to characterize AOT reverse micelles in isooctane and decane with several different polar solvents (formamide, ethylene glycol, acetonitrile, methanal, *N*,*N*-dimethylformamide, and 1,2-propanediol) as well as water. As the water content increases, the absorption spectrum shifts to the red and smoothly approaches that of bulk water. An interesting finding is that the character of these reverse micelles depends partially upon the solubility of the polar solvent in the hydrocarbon phase.

3.2. Continuum Models

Continuum models of electronic absorption spectra in bulk liquids have been used to derive expressions for the peak positions and width of the spectra in terms of the solvent dielectric properties and the solute properties.[12,28,66−68] The solute can be represented as a charge distribution (point charges or dipoles, etc.) inside a cavity or using a quantum description at varying levels of theory. Although continuum models of liquid interfaces have been used extensively to compute ionic solvation, adsorption free energy,[59,288−290] ionization energies,[291] and reorganization free energy,[292−296] there has been only one attempt to develop a simple continuum model of electronic absorption line shape at liquid interfaces.[297] We briefly describe the results of this study and some of its applications.

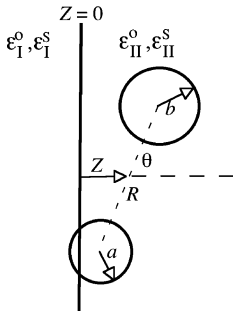

Figure 6. A schematic representation of the continuum electrostatic model for calculating the electronic absorption spectra at the liquid/liquid interface. The chromophore is represented by two spherical cavities of radii a and b at a distance R from each other and at a distance Z and orientation θ with respect to the interface. Equal size and opposite sign point charges are in the center of the two cavities. The electronic transition involves a change in the magnitude of the charge.

The calculations of the peak and line width of the absorption spectrum are based on linear response theory. The peak absorption spectrum shift relative to a vacuum is given by[12,297]

$$\Delta\omega_{abs} = \frac{1}{8\pi}\oint\oint\oint\{[\epsilon^o(\mathbf{E}^o_{ex} - \mathbf{E}^o_{gr})^2 - \epsilon^s(\mathbf{E}^s_{ex} - \mathbf{E}^s_{gr})^2] + \epsilon^s[\mathbf{E}^s_{ex}\cdot\mathbf{E}^s_{ex} - \mathbf{E}^s_{gr}\cdot\mathbf{E}^s_{gr}]\}\,d\mathbf{r} \quad (3.4)$$

where ϵ^o and ϵ^s are the optical and static dielectric constants of the medium, respectively, and $\mathbf{E}^m_\nu$ (m = o or s) is the electric field induced in this medium by the charge distribution of the νth electronic state. The calculation of the volume integrals in eq 3.4 is straightforward in a homogeneous medium and was carried out analytically for several different charge distributions.[12] To carry out these calculations at the interface, the chromophore is modeled as a finite-size dipole by a pair of nonoverlapping spherical cavities of radii a and b, in which two equal and opposite point charges are embedded: $\pm Q_{gr}$ in the ground electronic state and $\pm Q_{ex}$ in the excited state. The interface is modeled as a plane perpendicular to the Z-axis and located at $Z = 0$ separating two bulk homogeneous media. ϵ^m_I is the dielectric constant for medium I (which occupies the $Z < 0$ region), and ϵ^m_{II} is the dielectric constant for medium II. The two cavities may be at any orientation and location relative to the interface, including situations where one or both cavities intersect the $Z = 0$ plane (Figure 6). The electric fields in eq 3.4 are determined from the potential $\phi(\mathbf{r})$ generated by the charge distribution in each electronic state, using $\mathbf{E} = -\nabla\phi$. The potential due to a particular charge distribution can be written as a sum of the contributions from all point charges and from their images at the interface.[297,298]

The line shape $I_{abs}(\omega,Z,\theta)$ at each position Z of the center of charge of the solute relative to the interface and at each angle θ between the solute and the interface normal is given by a Gaussian (eq 2.2), whose peak position (eq 3.4) depends on Z and θ and whose width can be determined from the relation (assuming linear response)[12,297]

$$\sigma_a^2 = \sigma_e^2 = \frac{kT}{4\pi}\oint\oint\oint[\epsilon^o(\mathbf{E}^o_{ex} - \mathbf{E}^o_{gr})^2 - \epsilon^s(\mathbf{E}^s_{ex} - \mathbf{E}^s_{gr})^2]\,d\mathbf{r} \quad (3.5)$$

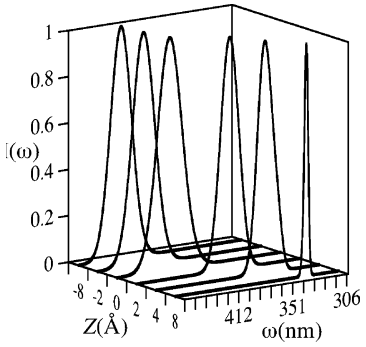

Figure 7. The orientationally averaged electronic absorption line shape of DEPNA at different locations at the water liquid/vapor interface, calculated using the continuum electrostatic model. The spectra are normalized at each position, and the frequency scale is linear in energy. Adapted from ref 297.

One may then calculate an orientationally averaged line shape by a proper Boltzmann weighting of $I_{abs}(\omega,Z,\theta)$. For additional details of the calculations and for an approximate analytical formula, see ref 297.

The above theory has been used to calculate the peak position of DEPNA at the air/water and water/1,2-dichloroethane (DCE) interface. The size of the two spherical cavities that reproduce the peak position of the experimental absorption line shape of DEPNA in bulk water is first calculated and found to be $a = b = 2.64$ Å at a distance of 6 Å apart. This structure is then kept fixed in all the spectra calculations at the interface. The values of the ground- and excited-state dipole moments of DEPNA are taken from a fit of molecular dynamics simulations to the experimental spectra in bulk water. The charges in the ground and excited states are then found to be $Q_{gr} = 0.35e$ and $Q_{ex} = 0.70e$, respectively. For the calculations at the water liquid/vapor interface, the dielectric constants of the two media used are $\epsilon^o_{liq} = 1.78$, $\epsilon^s_{liq} = 78$, $\epsilon^o_{vap} = \epsilon^s_{vap} = 1$, and for the calculations at the water/DCE interface they are $\epsilon^o_{DCE} = 2.5$ and $\epsilon^s_{DCE} = 10$. The temperature is $T = 298$ K.

The calculations of $I_{abs}(\omega,Z,\theta)$ at the air/water interface show that bulk behavior is already established 6 Å below the surface and that near the interface there is a strong orientation dependence. The solute "prefers" to be parallel to the interface when it is on the water side and perpendicular to the interface when it is on the vapor side, so these orientations will contribute more to the orientationally averaged line shape. This spectrum is shown in Figure 7 at $Z = -8$, -2, 0, 2, 4, and 8 Å. The spectrum in the bulk peaks at the value of $\omega_{max} = 428.4$ nm. This is the experimental value that the radius of the cavity is selected to reproduce. However, the half-width at half-height of the line shape is only $\Delta\omega = 18$ nm, compared with the experimental value of about $\Delta\omega = 30$ nm. This discrepancy is not surprising, since some broadening mechanisms (vibronic, lifetime) are left out from the treatment and higher order corrections are neglected in the expansion that leads to the Gaussian expression. As the solute approaches the interface, the peak spectrum shifts slowly to the blue, in agreement with experiments. Very close to the interface, the peak position is very sensitive to the location of the solute, which is a direct consequence of the discontinuous jump in the dielectric properties of the model. Because of this sensitivity, it is somewhat difficult to compare the result with the experimental value of $\omega_{max} = 377$ nm.[251] This value is reproduced if one takes the position of the chromophore to be $Z = 1.5$ Å, which is slightly into the vapor phase, consistent with the hydrophobic nature of the solute. Thus, the continuum model gives qualitatively reasonable results for the frequency shift of the electronic absorption spectrum.

In contrast, when the continuum model is applied to the water/DCE interface using the same solute parameter as above, the blue shift relative to bulk water is underestimated. This is because the stabilization of DEPNA in DCE is overestimated as a result of a too small cavity size. The cavity size is selected to match the spectrum in bulk water, and the different solvation structure of DEPNA in DCE must result in a larger cavity, as is confirmed in molecular dynamics simulations.[261] Indeed, in typical applications of continuum models to the calculation of electronic spectra, the cavity size is taken to be solvent-dependent. While it is possible to improve the results of the continuum model by selecting a larger cavity in DCE, to make the model consistent the cavity size must itself be a function of Z.

While the continuum electrostatic model discussed above provides a convenient qualitative approach for estimating interfacial effects on spectral line shapes and demonstrates the dependence of the spectra on interface location, it also underscores the problems inherent in continuum models of the interface. The model could be improved by introducing Z-dependent cavity size, more complicated cavity shapes, and surface roughness.

3.3. Computer Simulations

The methodology to compute the absorption spectrum within the Franck−Condon approximation was discussed in section 2.1. It has been used by many researchers to calculate absorption spectra in bulk liquids, and exactly the same procedure can be used at liquid interfaces. However, to date only a few calculations have been published.

Michael and Benjamin carried out a detailed study of DEPNA at the water/air and the water/DCE interfaces.[261] In addition to calculating several structural and dynamical properties of the system, the electronic absorption line shapes at the two interfaces were calculated. The potential energy functions used were typical for these types of simulations:

$$V_{gr} = V_{liq} + V_{LJ} + V^g_{el} + U^g_{pol}$$
$$V_{ex} = V_{liq} + V_{LJ} + V^e_{el} + U^e_{pol} + \Delta E_{gas} \qquad (3.6)$$

where V_{liq} is the potential energy function for the liquid molecules (a flexible SPC model[299,300] for water in the case of the liquid/vapor system and, in addition, a four-site model[140] for DCE in the case of the liquid/liquid interface), V_{LJ} is the total nonelectrostatic interaction between the solute's atoms and the liquid's atoms (assumed to be the same in the ground and excited states), V^g_{el} and V^e_{el} are the electrostatic interactions between the fixed point charges on the solute and the solvent atoms in the ground and excited states, respectively, and ΔE_{gas} is the fixed energy difference between the excited and ground electronic states of the solute in the gas phase. The atomic charges on DEPNA (*N*,*N*′-diethyl-*p*-nitroaniline) were selected with the aid of ab initio calculations, which were then adjusted to reproduce the ground-state dipole moment of DEPNA. The excited-state dipole moment was selected to fit the peak location of the bulk spectrum ($\mu_{ex} = 17$ D). This value was subsequently used without modification in the calculation of the electronic

spectra at the water liquid/vapor interface, in bulk DCE, and at the water/DCE interface.

Some of the calculations were done with polarizable potentials. In this case, the potential energy functions included the additional terms U_{pol}^{ν}, ν = g or e, which describe the electrostatic interactions between the induced dipoles on the atoms and other induced dipoles and fixed point charges for the solute in the electronic state ν. They are given by

$$U_{\mathrm{pol}}^{\nu} = -\frac{1}{2}\sum_{k}\mu_k^{\nu}\cdot\mathbf{E}_k^{\nu} \tag{3.7}$$

where μ_k^{ν} and $\mathbf{E}_k^{\nu}$ are, respectively, the induced electric dipole and the electric field vector at atomic site k when the solute is in the ν electronic state. The induced dipoles are calculated by iteratively solving at every step of the molecular dynamics simulation the equation

$$\mu_k^{\nu} = \alpha_k^{\nu}[\mathbf{E}_k^{\nu} - \sum_{l\neq k}\mathbf{T}_{kl}\cdot\mu_l^{\nu}] \tag{3.8}$$

where α_k^{ν} is the atomic polarizability of atomic site k and $\mathbf{T}$ is the dipole−dipole tensor:[301,302]

$$T_{kl} = \frac{3}{r_{kl}^{5}}\begin{pmatrix} x_{kl}^{2} & x_{kl}y_{kl} & x_{kl}z_{kl} \\ x_{kl}y_{kl} & y_{kl}^{2} & y_{kl}z_{kl} \\ x_{kl}z_{kl} & y_{kl}z_{kl} & z_{kl}^{2} \end{pmatrix} - \frac{1}{r_{kl}^{3}} \tag{3.9}$$

If the polarizable contributions are included, the fixed charges on the nonpolarizable liquid atoms are reduced to new values selected to give a reasonable description of the dielectric properties of the liquids. For example,[303] the charges of the nonpolarizable SPC model (0.41 au for the hydrogen and −0.82 au for the oxygen) were reduced to 0.365 au and −0.73 au, respectively, which reproduces the water gas-phase electric dipole moment of 1.86 D. Atomic polarizabilities were assigned, $\alpha_{\mathrm{H}} = 0.170$ Å^3 and $\alpha_{\mathrm{O}} = 0.528$ Å^3, which give rise to induced dipoles, which, together with the permanent dipole, approximately reproduce the total dipole moment of the nonpolarizable SPC model (2.3 D). The original paper should be consulted for the values of all these parameters for DCE.

The electronic absorption spectrum was calculated at the water liquid/vapor interface using a 1 ns simulation of a system that includes 1016 water molecules and one DEPNA. Figure 8 shows the results. Each spectral line is well described by a Gaussian curve (which, incidentally, demonstrates the quality of the second-order cumulant expansion discussed earlier). The excited-state dipole moment of DEPNA was chosen so that the peak position of its spectrum in bulk water agrees with the experimental value (429 nm). The half-width at half-height of the bulk spectrum was 34 nm, in good agreement with the experimental value of 37 nm,[251] suggesting that the pure inhomogeneous broadening assumption, inherent to the molecular dynamics calculations, is quite acceptable. Considering the experimental uncertainties and the very crude model used for the excited-state charge distribution in DEPNA, the calculated peak position of the spectrum at the water liquid/vapor interface was 382 nm, in reasonable agreement with the experimental value of 373 ± 4 nm.[251] The calculations at the water/DCE interface were done using a 1 ns simulation of a system that includes

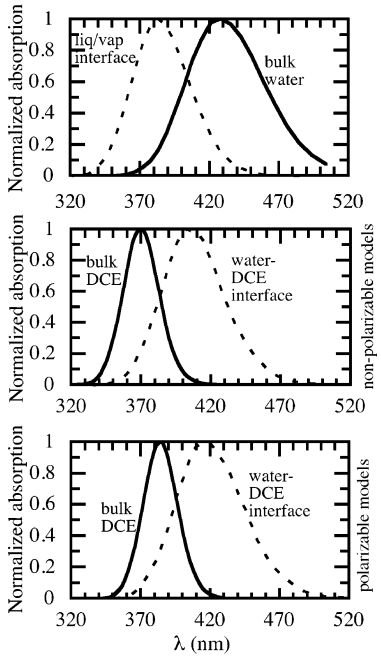

Figure 8. The electronic absorption line shape of DEPNA, calculated using molecular dynamics simulations at the water liquid/vapor interface (top panel) and at the nonpolarizable (middle panel) and polarizable (bottom panel) water/1,2-dichloroethane interface. Adapted from ref 261.

500 water molecules and 216 DCE molecules using the solute parameters from the liquid/vapor system without modifications. In this case, the agreement with experiment was quite poor. However, using a polarizable DCE potential significantly improved the results.

The reasonable agreement with experiments enables one to use the molecular dynamics results to gain insight into the reason for the peak of the interfacial spectrum to be near the average of the two bulk phases. One finds that although the water makes a larger contribution to the spectral shift due to its stronger interaction with the solute, it contributes 50% relative to the spectral shift in bulk water, mainly as a result of a depletion in the first hydration shell at the interface. A significant contribution to the polarity of the water/DCE interface was found to be due to the surface roughness, which enables the solute to interact with more water molecules relative to a situation where the surface is forced to remain flat.

Another conclusion of the above study has been that the main effect of introducing polarizable potentials is to increase the red shift (relative to the nonpolarizable model) by having much larger induced dipoles on the DCE molecules that are in the vicinity of the solute in its excited electronic state (which has larger charges).

In recent years, the importance of including many-body polarizable potentials in classical molecular dynamics simulations has received much attention.[37,71,148,302,304−315] The role of solvent and solute many-body polarizabilities in affecting the electronic absorption line shapes at the water liquid/vapor interface was examined by Benjamin[316] for a model dipolar solute using molecular dynamics computer simulations. The calculations included systematic variation of the solute excited-state dipole and polarizability and an examination of both polarizable and nonpolarizable water models. It was found that solvent polarizability has a more substantial effect on the peak absorption spectrum than solute polarizability.

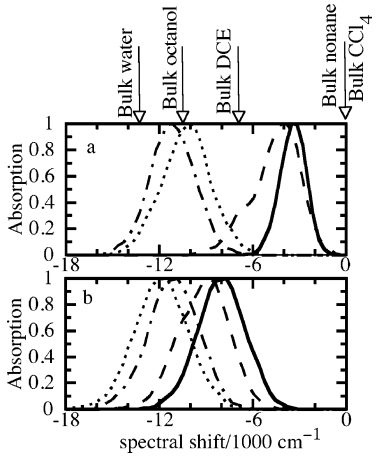

Figure 9. Electronic absorption spectra for a model electronic transition (dipole jump) at the interface between water and several organic liquids, calculated using molecular dynamics simulations. The top panel shows the results when the diatomic chromophore is located in the organic phase 5 Å from the Gibbs surface, and the arrows show the peak positions in the bulk organic liquids. In the bottom panel, the chromophore is located at the Gibbs surface. In each panel, the dotted, dashed−dotted, dashed, and solid lines are for DCE, octanol, CCl_4, and nonane, respectively. The spectral shift is relative to the gas phase. Adapted from ref 260 with permission. Copyright 1997 American Institute of Physics.

This effect was more pronounced as the excited-state dipole was increased and more in the bulk than at the interface.

A systematic study of the effect of the liquid/liquid interface locations, roughness, and polarity on electronic absorption line shape was reported by Michael and Benjamin.[260] A chromophore modeled as a dipolar solute with charges and Lennard-Jones parameters designed to approximately mimic DEPNA was inserted at two different locations at the interface between water and four different organic liquids representing various polarities and molecular shapes: 1-octanol, 1,2-DCE, *n*-nonane, and carbon tetrachloride. Some of the results are depicted in Figure 9. These spectra underscore the point that the effective polarity that the probe experiences depends not only on the polarity of the bulk liquids but also on the location and molecular shape of the organic liquid. Thus, for example, the water/CCl_4 interface is more polar than the water/nonane interface despite the fact that in these model calculations these two liquids are both purely nonpolar. This is due to the limited ability of water molecules to interact with the probe if it is buried in nonane, a long-chain alkane. In another demonstration of the importance of surface roughness, the calculations were repeated for water/1,2-DCE and water/CCl_4 interfaces while the interfaces were externally constrained to be smooth. Since the water/CCl_4 interface is already quite sharp, the spectrum is not affected, but in the case of DCE, the external flattening of the interface restricts the ability of water molecules to interact with the chromophore, which reduces the red shift. In both cases, the narrower spectral lines reflect the surface-reduced dynamics roughness. Some experimental support for the correlation between surface roughness and spectral width was reported by Walker and co-workers.[272−274] The above model was also used to test the continuum model discussed earlier. It was found that this model gives qualitatively reasonable results as far as the effect of interface polarity but is unable to reproduce the effect due to the probe location.

One difficulty in interpreting experiments carried out at liquid/liquid interfaces is the fact that the solute location is not known with precision and density fluctuations create additional uncertainty as to the local molecular environment. While this aspect of the liquid/liquid interface is an interesting feature that is currently under extensive study, it would be interesting to compare the electronic spectroscopy in this system to an interface where the structure is similar in the nature of the intermolecular interactions but structurally well-defined. One way to achieve this is to construct mimics of different water/organic liquid interfaces by chemically modifying the headgroups of hydrocarbon self-assembled monolayers (SAM). This enables one to study the direct relationship between a well-defined intrinsic structure and the dynamics and spectroscopy of adsorbed species. By varying the relative length of a mixture of hydrocarbon chains, one can also create a static roughness, which will enable its contribution to be distinguish from that due to the dynamic roughness at a normal liquid/liquid interface. Because the synthesis and characterization of SAM have seen explosive growth in recent years, the hope is that this will also stimulate new experiments along the lines of what is outlined below.

Benjamin and co-workers have used molecular dynamics computer simulations to study the structure, spectroscopy, and dynamics at the interface between water and simple hydrocarbon SAM with varying roughness as models for water/alkane liquid interfaces[317,318] and chlorinated SAM with varying degrees of chlorination and roughness as models for water/weakly polar liquid interfaces.[319] The structure of the simple hydrocarbon SAM, as well as its wetting behavior by water, was found to be in good agreement with experiments.[317] The electronic spectra of a chromophore attached to the interface between the SAMs and water have been examined by molecular dynamics computer simulations.[318] The electronic spectrum of the chromophore at the interface between the all-methyl-terminated SAM and water was found to be very similar to the spectrum calculated when the same chromophore is located at the water/nonane interface[260] with variations that are consistent with the structure of the interface and, in particular, the degree of exposure of the chromophore to interfacial water molecules. This also seems to correlate with the SHG measurements carried out by Walker and co-workers at the interface between water and hydrocarbon liquids.[273] The computed electronic absorption spectrum of an adsorbed chromophore at the chlorinated SAM/water interface shows[319] that the effective polarity of the interface is greater than that of bulk water, in contrast to the situation at several liquid/liquid interfaces but in agreement with recent experiments at the liquid/solid interface.[320,321] This higher effective polarity is shown to be due to a contribution from the polar groups at the surface that is larger than the loss due to the decreased interaction with water.

4. Solvation Dynamics at Liquid Interfaces

4.1. Experimental Data

In section 2.2, we discussed how time-resolved fluorescence spectroscopy can be used to study solvation dynamics in bulk liquids. Because the fluorescence signal from the bulk is typically much larger than that from the interface, this technique can be used to study solvation dynamics at liquid interfaces only if most of the probe molecules reside

at the interface. This is the case when the probe is strongly adsorbed at the interface (negligible solubility in the bulk of both phases) or when it is adsorbed at the micelle−liquid interface. Another possibility is to collect the fluorescence signal in total reflection geometry (this depends on the incident angle and the relative index of refraction of the two bulk media). This method has been used to measure solvation dynamics, but because the evanescent wave penetrates a few hundred angstroms beyond the surface, the surface selectivity is not clear. A promising method that is surface-selective is based on time-resolved resonance second harmonic generation. Below we summarize these approaches and the data obtained through them.

4.1.1. Time-Resolved Second Harmonic Generation Studies of Solvation Dynamics

Time-resolved SHG has been used by several workers to study a number of dynamical phenomena at interfaces.[110,111,252] The application to solvation dynamics was first reported by Eisenthal and co-workers.[53,55,322,323] The method involves three optical pulses: An optical pump pulse excites (some of) the molecules to an electronic excited state. A time-delayed probe pulse with a frequency ω generates a second harmonic pulse with frequency 2ω only from the interfacial molecules. As the solvent molecule reorganizes around the excited molecules, the energy difference between the ground and excited state varies. The quantity ω_{eg} in eq 3.2 becomes time-dependent for the excited molecules, and thus the resonant SH signal changes with the delay time. This change can be attributed to solvation dynamics if solute reorientation and ground-state recovery is much slower.[53,322] Since this experiment is done at a constant probe frequency, calculation of the correlation function, $S_\omega(t)$ (eq 2.4), requires repeating this measurement at many different frequencies. A simpler approach used by Eisenthal and co-workers is based on a linear wavelength procedure.[324] A single probe frequency is selected such that the resonant time-dependent second-order susceptibility, $|\chi_R^{(2)}|^2$, is proportional to $S_\omega(t)$.[53,322] The spectra at different times are related to the equilibrium spectra of a set of solvents, based on a polarity scale and the linear wavelength relationship.[85]

With the above method, the solvation dynamics of coumarin 314 (C314) adsorbed at the air/water interface was measured[322] and found to be very close to that in bulk water (0.8 ps). Since most of the hydration energy comes from the first coordination shell, this suggests that the hydration structure and dynamics of water molecules around the adsorbed solute in the excited state (which has a large dipole of 12 D) are similar to those in bulk water. This is consistent with molecular dynamics simulations to be discussed below.

Subsequent experiments with polarized pump pulses in the direction parallel and perpendicular to the interface showed that the solvation dynamics depend on the solute orientation. The solvation dynamics are faster around the solute when it is parallel to the interface.[53] This can be the result of several effects. Since the spectrum for the two orientations may be shifted (as demonstrated with the continuum model in section 3.2), monitoring the dynamics at one fixed wavelength could produce different decay constants.[53] It is also possible that the dynamics of water molecules are different for the two orientations, and molecular dynamics simulations could be helpful in this regard.

The effect of the external field on solvation dynamics at interfaces has been investigated by Benderskii et al. (Eisenthal group) utilizing C314 adsorbed at the air/water interface in the presence of neutral, anionic, and cationic surfactants.[55,323,325,326] Some of the data are summarized in Figure 10. The solvation dynamics measured using TRSHG were fitted to a double exponential, $S_\omega(t) \approx c_1\, e^{-t/\tau_1} + (1 - c_1)\, e^{-t/\tau_2}$, and the corresponding time constants and the amplitude of the fast component are shown in Figure 10 for the anionic (SDS) and cationic (CTAB) surfactants as a function of coverage and compared with the data in bulk water and the air/water interface with no surfactants. As the cationic surfactant surface density increases from 500 Å^2/molecule to 100 Å^2/molecule, the fast component slows from 380 (the value similar to that in bulk water and the air/water interface) to 550 fs, while its contribution increases from 75% to near 100%. The slow component is also slowed as the coverage increases, but because the amplitude becomes small, the errors are much larger. In contrast, the amplitude of the fast and slow components of the solvation dynamics in the presence of an anionic surfactant is nearly constant, and the effect on the relaxation time is not as dramatic. This suggests that the positive charge influences the water structure and dynamics to a greater degree. This is also reflected in the equilibrium absorption SHG spectra, which show a red shift and therefore increased local polarity at the positively charged interface ($\lambda_{max} = 436$ nm) compared with the surfactant-free air/water interface ($\lambda_{max} = 423$ nm), though they are less polar than bulk water ($\lambda_{max} = 448$ nm) but more polar than the negatively charged interfaces ($\lambda_{max} = 431-432$ nm).

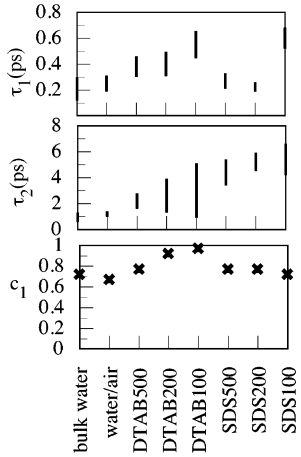

Figure 10. Double-exponential fitted parameters for the solvation dynamics of coumarin 314 in bulk water, at the air/water interface, and as a function of coverage of the anionic (SDS) and cationic (CTAB) surfactants. Data taken from Benderskii, A. V.; Eisenthal, K. B. *J. Phys. Chem. B.* **2004**, *108*, 3376.

The effect of external charges on water molecules at different interfaces has been extensively studied.[112,165,166,168,209−214] The opposite alignment of the water dipole next to positive or negative charges has a marked effect on the hydrogen-bonding network, and the above experiments show that there is also a significant effect on solvation dynamics.

4.1.2. Time-Resolved Total Internal Reflection Fluorescence

This technique has been used to study a number of interfacial dynamical phenomena. Applications to solvation dynamics include the following: (a) The solvation dynamics of coumarin 460 at the 1-butanol/sapphire interface was found to be much slower than that in bulk 1-butanol.[327] This

was interpreted to be due to strong hydrogen bonding between the liquid and the hydrophilic sapphire surface. (b) Teramae and co-workers compared the solvation dynamics of two different fluorofores at the water/heptane interface and in a heptane/ethanol mixture.[328] The relaxation time at the interface (270 ps) was similar to the one in the bulk mixture (200 ps), suggesting preferential hydration at the interface.

4.1.3. Solvation Dynamics in Micelles and Reverse Micelles

Solvation dynamics experiments in reverse micelles have been the subject of much recent interest. The work until the year 2000 has been reviewed by Nandi, Bhattacharyya, and Bagchi[57] and by Levinger.[62] The main goal of these studies was to characterize the dynamics of solvent molecules in confined geometries.[329] The experiments were typically done using time-resolved fluorescence, which, as explained earlier, does not have the sensitivity problem of planar liquid surfaces. The main result of these studies was the observation of a very slow relaxation component, hundreds of picoseonds, which is not present in the bulk liquid. This has been explained by the slow dynamics of solvent molecules bound to the surface of the reverse micelles, especially the hydrogen bonding of water to ionic headgroups. Most measurements have been carried out as a function of the size of the reverse micelles by varying the ratio of the polar liquid to the surfactant. For example, in the study of Levinger and co-workers on the solvation dynamics of coumarin 343 in the lecithin/water/cyclohexane reverse micelles,[330] at the smallest reverse micelle size all the water molecules are bound to the surface and one observes a slow 219 ps relaxation. As the water content increases and the reverse micelle increases in size, two other faster components appear, one of them similar to that of bulk water (0.4−0.6 ps) and the other representing a slow 14−17 ps relaxation also attributed to bulk water. For other examples published by the year 2000, one should consult the review articles listed at the top of this paragraph.[57,62]

In the past few years, the work in this area has explored in more detail the effect of size and shape of the micelles as well as the identity of the polar and nonpolar (continuous phase) liquids on the observed dynamics. Willard and Levinger studied the effect of a change in the morphology of the reverse micelle on the solvation dynamics.[331] They found that solvation dynamics of coumarin 343 in the spherical benzene/lecithin/water reverse micelles are faster than the dynamics in the tubular reverse micelle formed when the nonpolar phase is cyclohexane.

The solvation dynamics of coumarin 153 in water, methanol, and acetonitrile in *n*-heptane/AOT/water, *n*-heptane/AOT/methanol, and *n*-heptane/AOT/acetonitrile reverse micelles have been investigated by Hazra, Chakrabarty, and Sarkar using picosecond time-resolved emission spectroscopy.[332] Very slow dynamics on the order of a few nanoseconds were observed in all the three reverse micelles, compared to the pure solvents. However, while the solvation time is strongly dependent on the amount of the polar solvent in the case of water and methanol reverse micelles, very little dependency is observed in the case of acetonitrile reverse micelles. Similarly, Shirota and co-workers found that while the solvation dynamics of formamide in aerosol OT reverse micelles depend strongly on the molar ratio between formamide and aerosol OT, the solvation dynamics of *N*,*N*-dimethylformamide show a small dependence on the corresponding ratio.[333] Using ab initio calculations, they explained this in terms of different specific interactions between the polar solvent molecule and the polar headgroups of the surfactants.

While the focus of the solvation dynamics (and static spectra discussed in section 3.1) studies in reverse micelles has been the effect due to confinement, the insight gained about solute−solvent interactions at the interface between a polar and nonpolar phase is directly relevant to processes occurring at planar liquid/liquid and liquid/membrane interfaces. However, more directly related to the studies at planar interfaces are experiments done on micelles where the probe is adsorbed at the micelle/liquid interface. The dynamics of these systems is more closely related to the dynamics at the liquid/solid and liquid/membrane interfaces. The studies in these systems also observed significant slow dynamics compared with the dynamics in the bulk liquids. For example, the solvation dynamics of DCM (4-dicyanomethylene-2-methyl-6-*p*-dimethylaminostyryl-4*H*-pyran) have been studied in neutral (Triton X-100, TX), cationic (cetyl trimethylammonium bromide, CTAB), and anionic (sodium dodecyl sulfate, SDS) micelles using picosecond time-resolved Stokes shift. The time-dependent Stokes shift indicates that the water molecules in the Stern layer of the micelles relax on a time scale that is significantly slower than the subpicosecond relaxation dynamics in pure water.[334] In addition, the solvation dynamics in TX are slower than those in CTAB, and in all cases, they are multiexponential.[335] These data suggest that the slow dynamics are due to the strong interaction of water molecules with the surface of the micelles and that this interaction is (as expected) strongly dependent on the nature of the micelle headgroups, as was previously mentioned when we discussed the static spectra of these systems.

4.2. Computer Simulations

The experimental investigations of solvation dynamics at liquid interfaces described above are still clearly in the early stages, and much more work is expected soon. In contrast, molecular dynamics simulations have a longer history, because the methodology for conducting these calculations is essentially the same as that in the bulk. The goal of these simulations has been to understand the relationship between the structure of the interface and the static absorption spectra to the observed dynamics and to relate it to the properties of the neat interface.

In the absence of experimental data, the first solvation dynamics computer simulations at liquid interfaces were done on idealized model systems. Benjamin studied the solvation dynamics following the instantaneous creation of an ion at the water liquid/vapor interface.[258,300] The main finding was that the response in the bulk is almost identical to that at the interface. In both cases, there is a very rapid initial decay, which represents inertial solvent motion[22,23,33] and accounts for a slightly larger portion of the relaxation in bulk water, followed by a nearly exponential decay. An examination of the structure of the solvation complex[300] shows that the ion tends to keep its solvation shell intact and that this results in a similar dynamic response, since this response is mainly determined by the first solvation shell. This stability of the first solvation shell as the ion approaches the interface plays an important role in many other systems.[153]

Solvation dynamics at a model polar/nonpolar liquid/liquid interface were examined by Benjamin.[336] Both charge

separation and charge recombination processes in a diatomic probe oriented parallel or perpendicular to the interface were considered. The relaxation was found to be significantly slower at the interface compared to the bulk, especially for the charge separation process when the solute is perpendicular to the interface. This was found to be due to the large structural reorganization that must occur when a large dipole is created perpendicular to the interface. All the relaxation processes involve a significant initial fast inertial response that accounts for 40%−70% of the total relaxation. A detailed comparison with linear response shows that while the agreement between the nonequilibrium and equilibrium correlation functions is quite reasonable in the bulk and for the charge recombination process at the interface, a significant deviation from linear response is observed for the charge separation process. This is shown to be consistent with the large structural change observed during the nonequilibrium simulations.

The effect of solute location on solvation dynamics at the water/octanol interface was examined by Michael and Benjamin.[337] An instantaneous charge created at the water/octanol interface gave rise to a solvent response whose relaxation rate varied by 2 orders of magnitude depending on its location relative to the interface. This is reminiscent of experimental observations at the surface of micelles, but in the water/octanol case, the slow dynamics are related to the slow dynamics in bulk octanol, and the sharp change in the rate as a function of the probe location underscores the sharpness of the liquid/liquid interface.

A systematic study of solvation dynamics at different liquid/liquid interfaces was carried out by Michael and Benjamin.[338] The interfaces examined were between water and 1-octanol, 1,2-dichloroethane, *n*-nonane, and carbon tetrachloride, selected to give a range of polarity and interface structure. The electronic transitions involved a change in the permanent dipole of a dipolar solute located at the interface. Two locations of the solute relative to the interface were studied and compared with the same process in each of the bulk liquids. The solvent dynamic response at the interface was much more complex than that in the bulk. The relaxation involved a combination of the "bulklike" dynamics of both solvents and unique surface dynamics due to the existence of a sharp inhomogeneous boundary. The relative contribution of these different mechanisms depended on the location of the probe relative to the interface. As a result of these different contributions, the total relaxation involved multiple time scales corresponding to contributions from both solvents and the unique structural and dynamic properties of the interface. In particular, interfacial water relaxation may contain a slow component not present in the bulk nor at the water liquid/vapor interface. It was shown that this slow component corresponds to the very slow diffusion of finger-like water structures at the interface. Systems where these dynamics exist also exhibit marked deviations from linear response.

It is possible to explore the contribution of dynamic surface roughness at the liquid/liquid interface to the solvation dynamics by replacing the diffuse organic liquid with a SAM. To this end, the solvation dynamics following the electronic transition of a chromophore attached to the interface between water and SAM (whose spectra were discussed earlier) were examined by molecular dynamics simulations[318,339] and were compared with the same chromophore undergoing the same electronic transitions at the water/nonane and water/CCl_4 interfaces.[338] As expected, the very slow component found in the case of the probe located at the water/nonane and water/CCl_4 interfaces was missing from the corresponding interfaces between water and the methyl-terminated and chlorine-terminated SAMs, respectively. In addition, it was found that the solvation dynamics depend on both the roughness of the surface and its polarity and can be correlated with the shift in the electronic absorption spectra relative to those in bulk water. The dynamics are faster at the smooth surfaces and when the degree of chlorination is larger. By resolution of the relaxation into contributions from the water and the organic phase and by examination of these contributions as a function of the distance from the chromophore, it was found that most of the water contribution to the relaxation is due to water molecules in the first solvent shell. The tail of the relaxation is dominated by the slower dynamics of the chain molecules.

Pantano and Laria carried out molecular dynamics simulations of coumarin-314 at the water/air interface.[340] In addition to calculating a number of equilibrium and dynamical properties, they also studied the solvation dynamics following an excitation of the probe molecules. In agreement with the experiments of Eisenthal's group, the overall solvation dynamics was found to be only slightly slower at the interface (0.79 ps) than in the bulk (0.56 ps). The dynamics were characterized by an initial fast inertial drop that accounted for 50% of the overall relaxation in the bulk compared with 35% at the interface, similar to what was found in the studies reported above. Also in agreement with previous studies, the interfacial hydration structure was very similar to the one in the bulk, which again seems to account for the similar dynamics. They also computed the equilibrium time-correlation function (eq 2.6) and found excellent agreement with the nonequilibrium response, thus validating the linear response approximation in this case.

A molecular dynamics study of solvation dynamics in reverse micelles was reported by Faeder and Ladanyi.[341] They used a simple diatomic probe undergoing a charge localization jump ($-1/2, -1/2 \rightarrow -1, 0$) in model reverse micelles of varying size, and they compared the results to solvation dynamics of the probe in spherical cavities of the same size containing only water. They found that on the 0−2 ps time scale, the solvation response in reverse micelles becomes faster as the micelle size increases, in agreement with the experiments discussed above. Most of the slowing effect occurs in the slower, diffusive portion of the solvent response. In contrast, the short-time inertial dynamics, which account for over 70% of the response in all of the systems studied, appear to be independent of the system, even for the smallest size micelle. Calculations of the equilibrium solvation time-correlation functions demonstrate that the linear response approximation is accurate for these systems. An interesting point is that by decomposing the equilibrium response into pair and single-molecule contributions, they found that the collective contributions, which are faster than the single-molecule contribution, increase as the micelle size decreases. They also found that the relative magnitudes of fast (inertial) and slow (diffusive) contributions to the solvent response are sensitive to the location of the solute probe relative to the interface. This observation is similar to what was found in the simulation of solvation dynamics near self-assembled monolayers, as discussed above.

In a more recent contribution from Faeder and Ladanyi,[342] the effect of the headgroup charge on the solvation dynamics

was examined by switching the sign of the charge undergoing localization (thus the transition is $+^1/_2, +^1/_2 \rightarrow +1, 0$). They found that the solvation dynamics for the cationic chromophore are much slower and more strongly dependent on the size (or water content) of the model micelle. This difference was attributed, in part, to the different initial structure (location) of the probe, again in parallel to what was found in the case of self-assembled monolayers.

5. Conclusions and Outlook

The unique properties of the liquid interface region have a marked signature on the electronic absorption spectra and solvation dynamics of adsorbed dye molecules. In particular, the molecular structure of the solute−solvent complex and how it is affected by the anisotropic surface forces, by the different density and polarity, and by the dynamic surface roughness seem to be the most important factors determining the spectra and dynamics.

The experimental and theoretical studies of electronic spectra and solvation dynamics at liquid interfaces are still developing. While much has been learned from the work done in the past decade, there is still a need for new experimental data, especially on solvation dynamics, to provide more detailed and direct information about molecular interactions at the interface. Close collaboration between computer simulations and experiments will continue to be critical for future progress.

6. Acknowledgments

This work was supported by the National Science Foundation (Grant CHE-0345361). I would like to thank my collaborators: David Michael, Emilio Squitieri, Ilya Chorny, John Vieceli, and Nicole Winter. I am also grateful to Ken Eisenthal, Gil Nathanson, Rob Walker, and Mark Schlossmann for many discussions and help in understanding the intricacies of liquid interfaces.

7. References

(1) *The Chemistry of Acid Rain: Sources and Atmospheric Processes*; Johnson, R. W., Gordon, G. E., Eds.; American Chemical Society Symposium Series 349; American Chemical Society: Washington, DC, 1987.
(2) Finlayson-Pitts, B. J.; Pitts, J. N., Jr. *Chemistry of the Upper and Lower Atmosphere*; Academic Press: San Diego, CA, 2000.
(3) Starks, C. M.; Liotta, C. L.; Halpern, M. *Phase Transfer Catalysis*; Chapman & Hall: New York, 1994.
(4) Campbell, C. J.; Rusling, J. F. *Langmuir* **1999**, *15*, 7416.
(5) Makosza, M. *Pure Appl. Chem.* **2000**, *72*, 1399.
(6) Gennis, R. B. *Biomembranes*; Springer: New York, 1989.
(7) *Liquid−Liquid Interfaces*; Volkov, A. G., Deamer, D. W., Eds.; CRC press: Boca Raton, FL, 1996.
(8) *Interfacial Catalysis*; Volkov, A. G., Ed.; Marcel Dekker: New York, 2003.
(9) Bard, A. J.; Faulkner, L. R. *Electrochemical methods: fundamentals and applications*; Wiley: New York, 1980.
(10) Bockris, J. O. M.; Gonzalez-Martin, A. In *Spectroscopic and Diffraction Techniques in Interfacial Electrochemistry*; Gutierrez, C., Melendres, C., Eds.; Kluwer Academic Publishers: Dordrecht, The Netherlands 1990.
(11) Adamson, A. W. *Physical Chemistry of Surfaces*, 5th ed.; Wiley: New York, 1990.
(12) Marcus, R. A. *J. Chem. Phys.* **1965**, *43*, 1261.
(13) Mataga, N.; Kubota, T. *Molecular Interactions and Electronic Spectra*; Dekker: New York, 1970.
(14) Martire, B.; Gilbert, R. *Chem. Phys.* **1981**, *56*, 241.
(15) Zwan, G. v. d.; Hynes, J. T. *J. Chem. Phys.* **1983**, *78*, 4174.
(16) Wang, C. H. *Spectroscopy of condensed media*; Academic Press: New York, 1985.
(17) Fleming, G. R. *Chemical Applications of Ultrafast Spectroscopy*; Oxford University: New York, 1986.
(18) Hwang, J. K.; Creighton, S.; King, G.; Whitney, D.; Warshel, A. *J. Chem. Phys.* **1988**, *89*, 859.
(19) Maroncelli, M.; Castner, E. W., Jr.; Bagchi, B.; Fleming, G. R. *Faraday Discuss. Chem. Soc.* **1988**, *85*, 199.
(20) Rips, I.; Klafter, J.; Jortner, J. *J. Chem. Phys.* **1988**, *89*, 4288.
(21) Zhou, Y.; Friedman, H. L.; Stell, G. *J. Chem. Phys.* **1989**, *91*, 4885.
(22) Carter, E. A.; Hynes, J. T. *J. Chem. Phys.* **1991**, *94*, 5961.
(23) Chandra, A.; Bagchi, B. *J. Chem. Phys.* **1991**, *94*, 3177.
(24) Fonseca, T.; Ladanyi, B. M. *J. Phys. Chem.* **1991**, *95*, 2116.
(25) Maroncelli, M. *J. Chem. Phys.* **1991**, *94*, 2084.
(26) Raineri, F. O.; Zhou, Y.; Friedman, H. L.; Stell, G. *Chem. Phys.* **1991**, *152*, 201.
(27) Rosenthal, S. J.; Xie, X.; Du, M.; Fleming, G. R. *J. Chem. Phys.* **1991**, *95*, 4715.
(28) Ågren, H.; Mikkelsen, K. V. *J. Mol. Struct. (THEOCHEM)* **1991**, *234*, 425.
(29) Shemetulskis, N. E.; Loring, R. F. *J. Chem. Phys.* **1991**, *95*, 4756.
(30) Neria, E.; Nitzan, A. *J. Chem. Phys.* **1992**, *96*, 5433.
(31) Sarkar, N.; Datta, A.; Das, S.; Bhattacharyya, K. *J. Phys. Chem.* **1996**, *100*, 15483.
(32) Friedman, H. L.; Perng, B. C.; Resat, H.; Raineri, F. O. *J. Phys.: Condens. Matter* **1994**, *6* (S23), A131.
(33) Jimenez, R.; Fleming, G. R.; Kumar, P. V.; Maroncelli, M. *Nature* **1994**, *369*, 471.
(34) Skaf, M. S.; Ladanyi, B. M. *J. Phys. Chem.* **1996**, *100*, 18258.
(35) Song, X. Y.; Chandler, D.; Marcus, R. A. *J. Phys. Chem.* **1996**, *100*, 11954.
(36) Stratt, R. M.; Maroncelli, M. *J. Phys. Chem.* **1996**, *100*, 12981.
(37) Bader, J. S.; Berne, B. J. *J. Chem. Phys.* **1996**, *104*, 1293.
(38) Reichardt, C. *Chem. Rev.* **1994**, *94*, 2319.
(39) Suppan, P.; Ghoneim, N. *Solvatochromism*; The Royal Society of Chemistry: Cambridge, U.K., 1997.
(40) Stephens, M. D.; Saven, J. G.; Skinner, J. L. *J. Chem. Phys.* **1997**, *106*, 2129.
(41) Cichos, F.; Willert, A.; Rempel, U.; vonBorczyskowski, C. *J. Phys. Chem. A* **1997**, *101*, 8179.
(42) Egorov, S. A.; Stephens, N. D.; Skinner, J. L. *J. Chem. Phys.* **1997**, *107*, 10485.
(43) Datta, A.; Pal, S. K.; Mandal, D.; Bhattacharya, K. *J. Phys. Chem. B* **1998**, *102*, 6114.
(44) deBoeij, W. P.; M. S. Pshenichnikov; Wiersma, D. A. *Annu. Rev. Phys. Chem.* **1998**, *49*, 99.
(45) Ladanyi, B. M.; Maroncelli, M. *J. Chem. Phys.* **1998**, *109*, 3204.
(46) Mandal, D.; Datta, A.; Pal, S. K.; Bhattacharyya, K. *J. Phys. Chem. B* **1998**, *102*, 9070.
(47) Pant, D.; Riter, R. E.; Levinger, N. E. *J. Chem. Phys.* **1998**, *109*, 9995.
(48) Song, X. *J. Chem. Phys.* **1998**, *108*, 2594.
(49) Biswas, R.; Bagchi, B. *J. Phys. Chem. A* **1999**, *103*, 2495.
(50) Day, T. J. F.; Patey, G. N. *J. Chem. Phys.* **1999**, *110*, 10937.
(51) Shirota, H.; Horie, K. *J. Phys. Chem. B* **1999**, *103*, 1437.
(52) Tran, V.; Schwartz, B. J. *J. Phys. Chem. B* **1999**, *103*, 5570.
(53) Zimdars, D.; Eisenthal, K. B. *J. Phys. Chem. A* **1999**, *103*, 10567.
(54) Aherne, D.; Tran, V.; Schwartz, B. J. *J. Phys. Chem. B* **2000**, *104*, 5382.
(55) Benderskii, A. V.; Eisenthal, K. B. *J. Phys. Chem. B* **2000**, *104*, 11723.
(56) Geissler, P. L.; Chandler, D. *J. Chem. Phys.* **2000**, *113*, 9759.
(57) Nandi, N.; Bhattacharyya, K.; Bagchi, B. *Chem. Rev.* **2000**, *100*, 2013.
(58) Shen, Y. R. *The Principles of Nonlinear Optics*; Wiley: New York, 1984.
(59) Benjamin, I. In *Liquid−Liquid Interfaces*; Volkov, A. G., Deamer, D. W., Eds.; CRC Press: Boca Raton, FL, 1996.
(60) Benjamin, I. *Chem. Rev.* **1996**, *96*, 1449.
(61) Eisenthal, K. B. *J. Phys. Chem.* **1996**, *100*, 12997.
(62) Levinger, N. E. *Curr. Opin. Colloid Interface Sci.* **2000**, *5*, 118.
(63) Egorov, S. A.; Gallicchio, E.; Berne, B. J. *J. Chem. Phys.* **1997**, *107*, 9312.
(64) Egorov, S. A.; Rabani, E.; Berne, B. J. *J. Chem. Phys.* **1998**, *108*, 1407.
(65) Sevian, H. M.; Skinner, J. L. *J. Chem. Phys.* **1992**, *97*, 8.
(66) McRae, E. G. *J. Phys. Chem.* **1957**, *61*, 562.
(67) Bakhshiev, N. G. *Opt. Spektrosk.* **1964**, *16*, 821.
(68) Mirashi, L. S. P.; Kunte, S. S. *Spectrochim. Acta* **1989**, *45A*, 1147.
(69) Aaron, J. J.; Maafi, M.; Párkányi, C.; Boniface, C. *Spectrochim. Acta* **1995**, *51A*, 603.
(70) Chandler, D.; Schweizer, K. S.; Wolynes, P. G. *Phys. Rev. Lett.* **1982**, *49*, 1100.
(71) Chen, Y. C.; Lebowitz, J.; Nielaba, P. *J. Chem. Phys.* **1989**, *91*, 340.

(72) Kamlet, M. J.; Abboud, J. L.; Taft, R. W. In *Progress in Physical Organic Chemistry*; Cohen, S. G., Streitwieser, A., Taft, R. W., Eds.; Wiley: New York, 1981; Vol. 13.
(73) Reichardt, C. *Solvents and Solvent Effects in Organic Chemistry*, 2nd ed.; Springer-Verlag: Weinheim, Germany, 1988.
(74) Laurence, C.; Nicolet, P.; Dalati, M. T.; Abboud, J. L. M.; Notario, R. *J. Phys. Chem.* **1994**, *98*, 5807.
(75) Matyushov, D. V.; Schmid, R.; Ladanyi, B. M. *J. Phys. Chem. B* **1997**, *101*, 1035.
(76) Kim, H. J.; Hynes, J. T. *J. Chem. Phys.* **1990**, *93*, 5194.
(77) Kim, H. J.; Hynes, J. T. *J. Chem. Phys.* **1990**, *93*, 5211.
(78) Jacques, P. *J. Phys. Chem.* **1986**, *90*, 5535.
(79) Marcus, Y. *Chem. Soc. Rev.* **1993**, *22*, 409.
(80) Kamlet, M. J.; Taft, R. W. *J. Am. Chem. Soc.* **1976**, *98*, 377.
(81) Kamlet, M. J.; Hall, T. N.; Boykin, J.; Taft, R. W. *J. Org. Chem.* **1979**, *44*, 2599.
(82) Simon, J. D. *Acc. Chem. Res.* **1988**, *21*, 128.
(83) Barbara, P. F.; Jarzeba, W. *Adv. Photochem.* **1990**, *15*, 1.
(84) Cho, M.; Rosenthal, S. J.; Scherer, N. F.; Ziegler, L. D.; Fleming, G. R. *J. Chem. Phys.* **1992**, *96*, 5033.
(85) Gardecki, J. A.; Maroncelli, M. *Chem. Phys. Lett.* **1999**, *301*, 571.
(86) Frohlich, H. *Theory of dielectrics*; Clarendon: Oxford, U.K., 1958.
(87) Maroncelli, M.; Fleming, G. R. *J. Chem. Phys.* **1988**, *89*, 5044.
(88) Papazyan, A.; Maroncelli, M. *J. Chem. Phys.* **1993**, *98*, 6431.
(89) Maroncelli, M. *J. Mol. Liq.* **1993**, *57*, 1.
(90) Rossky, P. J.; Simon, J. D. *Nature* **1994**, *370*, 263.
(91) Ladanyi, B. M.; Stratt, M. *J. Phys. Chem.* **1996**, *100*, 1266.
(92) Wolynes, P. G. *J. Chem. Phys.* **1987**, *86*, 5133.
(93) Nichols, A. L.; Calef, D. F. *J. Chem. Phys.* **1988**, *89*, 3783.
(94) Bagchi, B. *Annu. Rev. Phys. Chem.* **1989**, *40*, 115.
(95) Walker, G. C.; Jarzeba, W.; Kang, T. J.; Johnson, A. E.; Barbara, P. F. *J. Opt. Soc. Am. B* **1990**, *7*, 1521.
(96) Kumar, P. V.; Maroncelli, M. *J. Chem. Phys.* **1995**, *103*, 3038.
(97) Fonseca, T.; Ladanyi, B. M. *J. Mol. Liq.* **1994**, *60*, 1.
(98) Petrov, N. K.; Wiessner, A.; Staerk, H. *J. Chem. Phys.* **1998**, *108*, 2326.
(99) Shirota, H.; Castner, E. W. *J. Chem. Phys.* **2000**, *112*, 2367.
(100) Luther, B. M.; Kimmel, J. R.; Levinger, N. E. *J. Chem. Phys.* **2002**, *116*, 3370.
(101) Pohorille, A.; Wilson, M. A. *J. Mol. Struct. (THEOCHEM)* **1993**, *103*, 271.
(102) Corn, R. M.; Higgins, D. A. *Chem. Rev.* **1994**, *94*, 107.
(103) Zhu, S.-B.; Singh, S.; Robinson, G. W. *Adv. Chem. Phys.* **1994**, *85*, 627.
(104) Benjamin, I. In *Modern Methods for Multidimensional Dynamics Computations in Chemistry*; Thompson, D. L., Ed.; World Scientific: Singapore, 1998.
(105) *Fluid Interfacial Phenomena*; Croxton, C. A., Ed.; Wiley: New York, 1986.
(106) *Spectroscopic and Diffraction Techniques in Interfacial Electrochemistry*; Gutierrez, C., Melendres, C., Eds.; NATO ASI Series, Vol. 320; Kluwer Academic Publishers: Dordrecht, The Netherlands, 1990.
(107) Mirkin, M. V.; Fan, F.-R. F.; Bard, A. J. *Science* **1992**, *257*, 364.
(108) Girault, H. H. In *Modern Aspects of Electrochemistry*; Bockris, J. O. M., Conway, B. E., White, R. E., Eds.; Plenum Press: New York, 1993; Vol. 25.
(109) Eisenthal, K. B. *Annu. Rev. Phys. Chem.* **1992**, *43*, 627.
(110) Brevet, P. F.; Girault, H. H. In *Liquid−Liquid Interfaces*; Volkov, A. G., Deamer, D. W., Eds.; CRC Press: Boca Raton, FL, 1996.
(111) Eisenthal, K. B. *Chem. Rev.* **1996**, *96*, 1343.
(112) Richmond, G. L. *Chem. Rev.* **2002**, *102*, 2693.
(113) Petersen, P. B.; Saykally, R. J. *J. Phys. Chem. B* **2005**, *109*, 7976.
(114) Petersen, P. B.; Saykally, R. J.; Mucha, M.; Jungwirth, P. *J. Phys. Chem. B* **2005**, *109*, 10915.
(115) Beaglehole, D. In *Fluid Interfacial Phenomena*; Croxton, C. A., Ed.; Wiley: New York, 1986.
(116) Pershan, P. S. *Faraday Discuss. Chem. Soc.* **1990**, *89*, 231.
(117) Penfold, J.; Thomas, R. K. *J. Phys. A: Condens. Matter* **1990**, *2*, 1369.
(118) Lee, L. T.; Langevin, D.; Farnoux, B. *Phys. Rev. Lett.* **1991**, *67*, 2678.
(119) Lee, L. T.; Langevin, D.; Mann, E. K.; Farnoux, B. *Physica B* **1994**, *198*, 83.
(120) Lu, J. R.; Thomas, R. K. *J. Chem. Soc., Faraday Trans.* **1998**, *94*, 995.
(121) Als-Nielsen, J. *Physica* **1986**, *140A*, 376.
(122) Schwartz, D. K.; Schlossman, M. L.; Kawamoto, E. H.; Kellogg, J. G.; Pershan, P. S.; Ocko, B. M. *Phys. Rev. A* **1990**, *41*, 5687.
(123) Sanyal, M. K.; Sinha, S. K.; Huang, K. G.; Ocko, B. M. *Phys. Rev. Lett.* **1991**, *66*, 628.
(124) Cowley, R. A. In *Equilibrium Structure and Properties of Surfaces and Interfaces*; Gonis, A., Stocks, G. M., Eds.; Plenum: New York, 1992.
(125) Pershan, P. S. *Physica A* **1996**, *231*, 111.
(126) Mitrinovic, D. M.; Zhang, Z.; Williams, S. M.; Huang, Z.; Schlossman, M. L. *J. Phys. Chem. B* **1999**, *103*, 1779.
(127) Schlossman, M. L. *Curr. Opin. Colloid Interface Sci.* **2002**, *7*, 235.
(128) Luo, G.; Malkova, S.; Pingali, S. V.; Schultz, D. G.; Lin, B.; Meron, M.; Graber, T. J.; Gebhardt, J.; Vanysek, P.; Schlossman, M. L. *Faraday Discuss.* **2005**, *129*, 23.
(129) Wirth, M. J.; Burbage, J. D. *J. Phys. Chem.* **1992**, *96*, 9022.
(130) Kovaleski, J. M.; Wirth, M. J. *J. Phys. Chem.* **1995**, *99*, 4091.
(131) Kuo, I. F. W.; Mundy, C. J. *Science* **2004**, *303*, 658.
(132) Croxton, C. A. *Statistical Mechanics of the Liquid Surface*; Wiley: New York, 1980.
(133) Rowlinson, J. S.; Widom, B. *Molecular Theory of Capillarity*; Clarendon: Oxford, U.K., 1982.
(134) Percus, J. K.; Williams, G. O. In *Fluid Interfacial Phenomena*; Croxton, C. A., Ed.; Wiley: New York, 1986.
(135) *Fundamentals of Inhomogeneous Fluids*; Henderson, D., Ed.; Marcel Dekker: New York, 1992.
(136) Napari, I.; Laaksonen, A.; Talanquer, V.; Oxtoby, D. W. *J. Chem. Phys.* **1999**, *110*, 5906.
(137) Conway, B. E. In *The Liquid State and its Electrical Properties*; Kunhardt, E. E., Christophorou, L. G., Luessen, L. H., Eds.; Nato ASI Series B, Vol. 193; Plenum: New York, 1988.
(138) Nicholson, D.; Parsonage, N. G. *Computer Simulation and the Statistical Mechanics of Adsorption*; Academic Press: New York, 1982.
(139) Linse, P. *J. Chem. Phys.* **1987**, *86*, 4177.
(140) Benjamin, I. *J. Chem. Phys.* **1992**, *97*, 1432.
(141) Iwamatsu, M. *J. Phys. Soc. Jpn.* **1991**, *60*, 1272.
(142) Gomez, M. A.; Chacon, E. *Phys. Rev. B* **1992**, *46*, 723.
(143) Kambayashi, S.; Chihara, J. *Mol. Simul.* **1996**, *16*, 31.
(144) Chekmarev, D.; Zhao, M.; Rice, S. A. *J. Chem. Phys.* **1998**, *109*, 768.
(145) Vanbuuren, A. R.; Marrink, S. J.; Berendsen, H. J. C. *J. Phys. Chem.* **1993**, *97*, 9206.
(146) Michael, D.; Benjamin, I. *J. Phys. Chem.* **1995**, *99*, 1530.
(147) Toxvaerd, S.; Stecki, J. *J. Chem. Phys.* **1995**, *102*, 7163.
(148) Chang, T. M.; Dang, L. X. *J. Chem. Phys.* **1996**, *104*, 6772.
(149) Michael, D.; Benjamin, I. *J. Electroanal. Chem.* **1998**, *450*, 335.
(150) Jedlovszky, P.; Vincze, Á.; Horvai, G. *J. Chem. Phys.* **2002**, *117*, 2271.
(151) Buff, F. P.; Lovett, A. A.; Stillinger, F. H. *Phys. Rev. Lett.* **1965**, *15*, 621.
(152) Deleted in proof.
(153) Benjamin, I. *Annu. Rev. Phys. Chem.* **1997**, *48*, 401.
(154) Mitrinovic, D. M.; Tikhonov, A. M.; Li, M.; Huang, Z.; Schlossman, M. L. *Phys. Rev. Lett.* **2000**, *85*, 582.
(155) Senapati, S.; Berkowitz, M. L. *Phys. Rev. Lett.* **2001**, *8717*, 6101.
(156) Weeks, J. D. *J. Chem. Phys.* **1977**, *67*, 3106.
(157) Weeks, J. D.; Vansaarloos, W.; Bedeaus, D.; Blokhuis, E. *J. Chem. Phys.* **1989**, *91*, 6494.
(158) Weeks, J. D. *J. Stat. Phys.* **1991**, *64*, 823.
(159) Pangali, C.; Rao, M.; Berne, B. J. *J. Chem. Phys.* **1979**, *71*, 2975.
(160) Lee, C. Y.; McCammon, J. A.; Rossky, P. J. *J. Chem. Phys.* **1984**, *80*, 4448.
(161) Spohr, E.; Heinzinger, K. *J. Chem. Phys.* **1986**, *84*, 2304.
(162) Spohr, E.; Heinzinger, K. *Ber. Bunsen-Ges. Phys. Chem.* **1988**, *92*, 1358.
(163) Spohr, E. *J. Phys. Chem.* **1989**, *93*, 6171.
(164) Rossky, P. J.; Lee, S. H. *Chem. Scr.* **1989**, *29A*, 93.
(165) Hautman, J.; Halley, J. W.; Rhee, Y.-J. *J. Chem. Phys.* **1989**, *91*, 467.
(166) Nagy, G.; Heinzinger, K. *J. Electroanal. Chem.* **1990**, *296*, 549.
(167) Heinzinger, K. *Pure Appl. Chem.* **1991**, *63*, 1733.
(168) Watanabe, M.; Brodsky, A. M.; Reinhardt, W. P. *J. Phys. Chem.* **1991**, *95*, 4593.
(169) Raghavan, K.; Foster, K.; Motakabbir, K.; Berkowitz, M. *J. Chem. Phys.* **1991**, *94*, 2110.
(170) Sullivan, D. E.; Levesque, D.; Weis, J. J. *J. Chem. Phys.* **1980**, *72*, 1170.
(171) Lee, L. L. *Molecular Thermodynamics of Nonideal Fluids*; Butterworth: Boston, MA, 1988.
(172) Horn, R. G.; Israelachvili, J. N. *J. Chem. Phys.* **1981**, *75*, 1400.
(173) Israelachvili, J. N. *Adv. Colloid Interface Sci.* **1982**, *16*, 31.
(174) Israelachvili, J. N. *Intermolecular and Surfaces Forces*; Academic Press: London, 1992.
(175) Derjaguin, B. V.; Churaev, N. V. In *Fluid Interfacial Phenomena*; Croxton, C. A., Ed.; Wiley: New York, 1986.
(176) Benjamin, I. *Science* **1993**, *261*, 1558.

(177) Schweighofer, K. J.; Benjamin, I. *J. Phys. Chem.* **1995**, *99*, 9974.
(178) Schweighofer, K. J.; Benjamin, I. *J. Phys. Chem. A* **1999**, *103*, 10274.
(179) Dang, L. X. *J. Phys. Chem. B* **1999**, *103*, 8195.
(180) dos Santos, D. J.; Gomes, J. A. *ChemPhysChem* **2002**, *3*, 946.
(181) Kornyshev, A. A.; Kuznetsov, A. M.; Urbach, M. *J. Chem. Phys.* **2002**, *117*, 6766.
(182) Wardle, K. E.; Carlson, E.; Henderson, D.; Rowley, R. L. *J. Chem. Phys.* **2004**, *120*, 7681.
(183) Benjamin, I. In *Structure and Reactivity in Aqueous Solution*; Cramer, C. J., Truhlar, D. G., Eds.; ACS Symposium Series 568; American Chemical Society: Washington, DC, 1994.
(184) King, M. E.; Nathanson, G. M.; Hanning-Lee, M. A.; Minton, T. K. *Phys. Rev. Lett.* **1993**, *70*, 1026.
(185) Nathanson, G. M.; Davidovitz, P.; Worsnop, D. R.; Kolb, C. E. *J. Phys. Chem.* **1996**, *100*, 13007.
(186) Chorny, I.; Benjamin, I.; Nathanson, G. M. *J. Phys. Chem. B* **2004**, *108*, 995.
(187) Lipkin, N.; Gerber, R. B.; Moiseyev, N.; Nathanson, G. M. *J. Chem. Phys.* **1994**, *100*, 8408.
(188) Benjamin, I.; Wilson, M. A.; Pohorille, A. *J. Chem. Phys.* **1994**, *100*, 6500.
(189) Benjamin, I.; Wilson, M. A.; Pohorille, A.; Nathanson, G. M. *Chem. Phys. Lett.* **1995**, *243*, 222.
(190) Taylor, R. S.; Dang, L. X.; Garrett, B. C. *J. Phys. Chem. B* **1996**, *100*, 11720.
(191) Fernandes, P. A.; Cordeiro, M. N. D. S.; Gomes, J. A. N. F. *J. Phys. Chem. B* **1999**, *103*, 6290.
(192) Chen, B.; Siepmann, J. I.; Klein, M. L. *J. Am. Chem. Soc.* **2002**, *124*, 12232.
(193) Chang, T.-M.; Dang, L. X. *J. Phys. Chem. B* **2005**, *109*, 5759.
(194) Heinz, T. F.; Tom, H. W. K.; Shen, Y. R. *Phys. Rev. A* **1983**, *28*, 1883.
(195) Goh, M. C.; Hicks, J. M.; Kemnitz, K.; Pinto, G. R.; Bhattacharyya, K.; Eisenthal, K. B.; Heinz, T. F. *J. Phys. Chem.* **1988**, *92*, 5074.
(196) Grubb, S. G.; Kim, M. W.; Raising, T.; Shen, Y. R. *Langmuir* **1988**, *4*, 452.
(197) Higgins, D. A.; Naujok, R. R.; Corn, R. M. *Chem. Phys. Lett.* **1993**, *213*, 485.
(198) Naujok, R. R.; Higgins, D. A.; Hanken, D. G.; Corn, R. M. *J. Chem. Soc., Faraday Trans.* **1995**, *91*, 1411.
(199) Eisert, F.; Dannenberger, O.; Buck, M. *Phys. Rev. B* **1998**, *58*, 10860.
(200) Lu, R.; Gan, W.; Wu, B. H.; Chen, H.; Wang, H. F. *J. Phys. Chem. B* **2004**, *108*, 7297.
(201) Goh, M. C.; Eisenthal, K. B. *Chem. Phys. Lett.* **1989**, *157*, 101.
(202) Du, Q.; Superfine, R.; Freysz, E.; Shen, Y. R. *Phys. Rev. Lett.* **1993**, *70*, 2313.
(203) Du, Q.; Freysz, E.; Shen, Y. R. *Science* **1994**, *264*, 826.
(204) Raymond, E. A.; Tarbuck, T. L.; Brown, M. G.; Richmond, G. L. *J. Phys. Chem. B* **2003**, *107*, 546.
(205) Richmond, G. L. *Annu. Rev. Phys. Chem.* **2001**, *52*, 257.
(206) Scatena, L. F.; Richmond, G. L. *Science* **2001**, *292*, 908.
(207) Brown, M. G.; Walker, D. S.; Raymond, E. A.; Richmond, G. L. *J. Phys. Chem. B* **2003**, *107*, 237.
(208) Walker, D. S.; Brown, M. G.; McFearin, C. L.; Richmond, G. L. *J. Phys. Chem. B* **2004**, *108*, 2111.
(209) Xia, X.; Berkowitz, M. L. *Phys. Rev. Lett.* **1995**, *74*, 3193.
(210) Schweighofer, K. J.; Benjamin, I. *J. Electroanal. Chem.* **1995**, *391*, 1.
(211) Benjamin, I. In *Modern Aspects of Electrochemistry*; Bockris, J. O. M., Conway, B. E., White, R. E., Eds.; Plenum Press: New York, 1997; Vol. 31.
(212) Ong, S.; Zhao, X.; Eisenthal, K. B. *Chem. Phys. Lett.* **1992**, *191*, 327
(213) Zhao, X. L.; Ong, S. W.; Eisenthal, K. B. *Chem. Phys. Lett.* **1993**, *202*, 513.
(214) Becraft, K. A.; Moore, F. G.; Richmond, G. L. *J. Phys. Chem. B* **2003**, *107*, 3675.
(215) Wilson, K. R.; Rude, B. S.; Catalano, T.; Schaller, R. D.; Tobin, J. G.; Co, D. T.; Saykally, R. J. *J. Phys. Chem. B* **2001**, *105*, 3346.
(216) Wilson, M. A.; Pohorille, A.; Pratt, L. R. *J. Phys. Chem.* **1987**, *91*, 4873
(217) Matsumoto, M.; Kataoka, Y. *J. Chem. Phys.* **1989**, *90*, 2398.
(218) Du, Q.; Freysz, E.; Shen, Y. R. *Phys. Rev. Lett.* **1994**, *72*, 238.
(219) Miranda, P. B.; Shen, Y. R. *J. Phys. Chem. B* **1999**, *103*, 3292.
(220) Shultz, M. J.; Baldelli, S.; Schnitzer, C.; Sitnonell, D. *J. Phys. Chem. B* **2002**, *106*, 5313.
(221) Morita, A.; Hynes, J. T. *Chem. Phys.* **2000**, *258*, 371.
(222) Yeh, Y. L.; Zhang, C.; Held, H.; Mebel, A. M.; Wei, X.; Lin, S. H.; Shen, Y. R. *J. Chem. Phys.* **2001**, *114*, 1837.
(223) Morita, A.; Hynes, J. T. *J. Phys. Chem. B* **2002**, *106*, 673.
(224) Perry, A.; Ahlborn, H.; Space, B.; Moore, P. B. *J. Chem. Phys.* **2003**, *118*, 8411.
(225) Jorgensen, W. L.; Chandresekhar, J.; Madura, J. D.; Impey, R. W.; Klein, M. L. *J. Chem. Phys.* **1983**, *79*, 926.
(226) Gao, J.; Jorgensen, W. L. *J. Phys. Chem.* **1988**, *92*, 5813.
(227) Luzar, A.; Chandler, D. *Nature* **1996**, *379*, 55.
(228) Starr, F. W.; Nielsen, J. K.; Stanley, H. E. *Phys. Rev. E: Stat. Phys. Plasmas, Fluids, Relat. Interdiscip. Top.* **2000**, *62*, 579.
(229) Luzar, A. *J. Chem. Phys.* **2000**, *113*, 10663.
(230) Balasubramanian, S.; Pal, S.; Bagchi, B. *Phys. Rev. Lett.* **2002**, *89*, 115505/1.
(231) Tarek, M.; Tobias, D. J. *Phys. Rev. Lett.* **2002**, *88*, 138101.
(232) Lopez, C. F.; Nielsen, S. O.; Klein, M. L.; Moore, P. B. *J. Phys. Chem, B* **2004**, *108*, 6603.
(233) Benjamin, I. *J. Phys. Chem. B* **2005**, *109*, 13711.
(234) Liu, P.; Harder, E.; Berne, B. J. *J. Phys. Chem. B* **2005**, *109*, 2949.
(235) Vanderham, E. W. M.; Vrehen, Q. H. F.; Eliel, E. R. *Surf. Sci.* **1996**, *368*, 96.
(236) Hommel, E. L.; Ma, G.; Allen, H. C. *Anal. Sci.* **2001**, *17*, 1325.
(237) Liu, P.; Harder, E.; Berne, B. J. *J. Phys. Chem. B* **2004**, *108*, 6595.
(238) *Molecular Dynamics in Restricted Geometries*; Klafter, J.; Drake, J. M., Eds.; Wiley: New York, 1989.
(239) Granick, S. *Science* **1991**, *253*, 1374.
(240) Lee, S. H.; Rossky, P. J. *J. Chem. Phys.* **1994**, *100*, 3334.
(241) Steele, W. A. *Adv. Chem. Phys.* **1976**, *34*, 1.
(242) Balucani, U.; Zoppi, M. *Dynamics of the Liquid State*; Clarendon Press: Oxford, U.K., 1994.
(243) Spohr, E. *Chem. Phys.* **1990**, *141*, 87.
(244) Nienhuys, H.-K.; Santen, R. A. v.; Bakker, H. J. *J. Chem. Phys.* **2000**, *112*, 8487.
(245) Faeder, J.; Ladanyi, B. M. *J. Phys. Chem. B* **2000**, *104*, 1033.
(246) Harpham, M. R.; Ladanyi, B. M.; Levinger, N. E.; Herwig, K. W. *J. Chem. Phys.* **2004**, *121*, 7855.
(247) Pollack, E. L.; Alder, B. J. *Annu. Rev. Phys. Chem.* **1981**, *32*, 311.
(248) *Water: A comprehensive Treatise*; Franks, F., Ed.; Plenum: New York, 1982; Vol. 4.
(249) *The Chemical Physics of Solvation, part C*; Dogonadze, R. R., Kalman, E., Kornyshev, A. A., Ulstrup, J., Eds.; Elsevier: Amsterdam, 1988.
(250) Kuznetsov, A. M. *Charge Transfer in Physics, Chemistry and Biology*; Gordon and Breach: Amsterdam, 1995.
(251) Wang, H.; Borguet, E.; Eisenthal, K. B. *J. Phys. Chem. A* **1997**, *101*, 713.
(252) Meech, S. R.; Yoshihara, K. *Chem. Phys. Lett.* **1990**, *174*, 423.
(253) Conboy, J. C.; Daschbach, J. L.; Richmond, G. L. *J. Phys. Chem.* **1994**, *98*, 9688.
(254) Conboy, J. C.; Daschbach, J. L.; Richmond, G. L. *Appl. Phys. A* **1994**, *59*, 623.
(255) Conboy, J. C.; Richmond, G. L. *Electrochim. Acta* **1995**, *40*, 2881.
(256) Essfar, M.; Guiheneuf, G.; Abboud, J. M. *J. Am. Chem. Soc.* **1982**, *104*, 6786.
(257) Wang, H. F.; Borguet, E.; Eisenthal, K. B. *J. Phys. Chem. B* **1998**, *102*, 4927.
(258) Benjamin, I. In *Reaction Dynamics in Clusters and Condensed Phases*; Jortner, J., Levine, R. D., Pullman, B., Eds.; Kluwer: Dordrecht, The Netherlands, 1994.
(259) Chandler, D. *Introduction to Modern Statistical Mechanics*; Oxford University Press: Oxford, U.K., 1987.
(260) Michael, D.; Benjamin, I. *J. Chem. Phys.* **1997**, *107*, 5684.
(261) Michael, D.; Benjamin, I. *J. Phys. Chem. B* **1998**, *102*, 5145.
(262) Tamburello-Luca, A. A.; Hébert, P.; Antoine, R.; Brevet, P. F.; Girault, H. H. *Langmuir* **1997**, *13*, 4428.
(263) Steel, W. H.; Walker, R. A. *J. Am. Chem. Soc.* **2003**, *125*, 1132.
(264) Tamburello-Luca, A. A.; Hébert, P.; Brevet, P. F.; Girault, H. H. *J. Chem. Soc., Faraday Trans.* **1996**, *92*, 3079.
(265) Pohorille, A.; Benjamin, I. *J. Chem. Phys.* **1991**, *94*, 5599.
(266) Nagatani, H.; Piron, A.; Brevat, P. F.; Fermin, D. J.; Girault, H. H. *Langmuir* **2002**, *18*, 6647.
(267) Suslick, K. S.; Chen, C. T.; Meredith, G. R.; Cheng, L. T. *J. Am. Chem. Soc.* **1992**, *114*, 6928.
(268) Levinger, N. E.; Kung, K. Y.; Luther, B. M.; Willard, D. M. In *Laser Techniques for Surface Science II*; Hicks, J. M., Ho, W., Dai, H.-L., Eds.; SPIE: Bellingham, WA, 1995; Vol. 2547.
(269) Uchida, T.; Yamaguchi, A.; Ina, T.; Teramae, N. *J. Phys. Chem. B* **2000**, *104*, 12091.
(270) Steinhurst, D. A.; Owrutsky, J. C. *J. Phys. Chem. B* **2001**, *105*, 3062.
(271) Steel, W. H.; Nolan, R.; Damkaci, F.; Walker, R. A. *J. Am. Chem. Soc.* **2002**, *124*, 4824.
(272) Steel, W. H.; Walker, R. A. *Nature* **2003**, *424*, 296.
(273) Steel, W. H.; Lau, Y. Y.; Beildeck, C. L.; Walker, R. A. *J. Phys. Chem. B* **2004**, *108*, 13370.
(274) Steel, W. H.; Beildeck, C. L.; Walker, R. A. *J. Phys. Chem. B* **2004**, *108*, 16107.
(275) Schlossman, M. L.; Li, M.; Mitrinovic, D. M.; Tikhonov, A. M. *High Perform. Polym.* **2000**, *12*, 551.

(276) Benjamin, I. *Chem. Phys. Lett.* **2004**, *393*, 453.
(277) Beildeck, C. L.; Steel, W. H.; Walker, R. A. *Langmuir* **2003**, *19*, 4933.
(278) Beildeck, C. L.; Steel, W. H.; Walker, R. A. *Faraday Discuss.* **2005**, *129*, 69.
(279) Kalyanasundaram, K. *Photochemistry in Microheterogenous Systems*; Academic Press: Orlando, FL, 1987.
(280) *Structure and Reactivity in Reverse Micelles*; Pileni, M. P., Ed.; Elsevier: Amsterdam, 1989.
(281) Saroja, G.; Samanta, A. *Chem. Phys. Lett.* **1995**, *246*, 506.
(282) Kalyanasundaram, K.; Thomas, J. K. *J. Am. Chem. Soc.* **1977**, *99*, 2039.
(283) Kalyanasundaram, K.; Thomas, J. K. *J. Phys. Chem.* **1977**, *81*, 2176.
(284) Laia, C. A. T.; Costa, S. M. B. *Phys. Chem. Chem. Phys.* **1999**, *1*, 4409.
(285) Vitha, M. F.; Weckwerth, J. D.; Odland, K.; Dema, V.; Carr, P. W. *J. Phys. Chem.* **1996**, *100*, 18823.
(286) Vitha, M. F.; Carr, P. W. *J. Phys. Chem. B* **1998**, *102*, 1888.
(287) Riter, R. E.; Kimmel, J. R.; Undiks, E. P.; Levinger, N. E. *J. Phys. Chem. B* **1997**, *101*, 8292.
(288) Kharkats, Y. I. *Elektrokhimiya* **1979**, *15*, 409.
(289) *The Chemical Physics of Solvation, part A*; Dogonadze, R. R., Kalman, E., Kornyshev, A. A., Ulstrup, J., Eds.; Elsevier: Amsterdam, 1985.
(290) Ulstrup, J.; Kharkats, Y. I. *Elektrokhimiya* **1993**, *29*, 299.
(291) Makov, G.; Nitzan, A. *J. Phys. Chem.* **1994**, *98*, 3459.
(292) Kharkats, Y. I.; Volkov, A. G. *J. Electroanal. Chem.* **1985**, *184* 435.
(293) Kuznetsov, A. M.; Kharkats, Y. I. In *The Interface Structure and Electrochemical Processes at the Boundary Between Two Immiscible Liquids*; Kazarinov, V. E., Ed.; Springer: Berlin, 1987.
(294) Kharkats, Y. I.; Ulstrup, J. *Chem. Phys.* **1990**, *141*, 117.
(295) Marcus, R. A. *J. Phys. Chem.* **1990**, *94*, 1050.
(296) Benjamin, I.; Kharkats, Y. I. *Electrochim. Acta* **1998**, *44*, 133.
(297) Benjamin, I. *J. Phys. Chem. A* **1998**, *102*, 9500.
(298) Jackson, J. D. *Classical Electrodynamics*; Wiley: New York, 1963.
(299) Berendsen, H. J. C.; Postma, J. P. M.; Gunsteren, W. F. V.; Hermans, J. In *Intermolecular Forces*; Pullman, B., Ed.; D. Reidel: Dordrecht, The Netherlands, 1981.
(300) Benjamin, I. *J. Chem. Phys.* **1991**, *95*, 3698.
(301) Vesely, F. J. *J. Comput. Phys.* **1977**, *24*, 361.
(302) Ahlstrom, P.; Wallqvist, A.; Engstrom, S.; Jonsson, B. *Mol. Phys.* **1989**, *68*, 563.
(303) Dang, L. X. *J. Chem. Phys.* **1992**, *97*, 2659.
(304) Sprik, M.; Klein, M. L. *J. Chem. Phys.* **1988**, *89*, 7556.
(305) Wallqvist, A. *Chem. Phys. Lett.* **1990**, *165*, 437.
(306) Wallqvist, A. *Chem. Phys.* **1990**, *148*, 439.
(307) Dang, L. X.; Rice, J. E.; Caldwell, J.; Kollman, P. A. *J. Am. Chem. Soc.* **1991**, *113*, 2481.
(308) Motakabbir, K.; Berkowitz, M. *Chem. Phys. Lett.* **1991**, *176*, 61.
(309) Karim, O. A. *J. Chem. Phys.* **1992**, *96*, 9237.
(310) Smith, D. E.; Dang, L. X. *J. Chem. Phys.* **1994**, *100*, 3757.
(311) Tsun-Mei, C.; Dang, L. X.; Peterson, K. A. *J. Phys. Chem. B* **1997**, *101*, 3413.
(312) Jungwirth, P.; Tobias, D. J. *J. Phys. Chem. A* **2002**, *106*, 379.
(313) Small, D. W.; Matyushov, D. V.; Voth, G. A. *J. Am. Chem. Soc.* **2003**, *125*, 7470.
(314) Salvador, P.; Curtis, J. E.; Tobias, D. J.; Jungwirth, P. *Phys. Chem. Chem. Phys.* **2003**, *5*, 3752.
(315) Vrbka, L.; Mucha, M.; Minofar, B.; Jungwirth, P.; Brown, E. C.; Tobias, D. J. *Curr. Opin. Colloid Interface Sci.* **2004**, *9*, 67.
(316) Benjamin, I. *Chem. Phys. Lett.* **1998**, *287*, 480.
(317) Rudich, Y.; Benjamin, I.; Naaman, R.; Thomas, E.; Trakhtenberg, S.; Ussyshkin, R. *J. Phys. Chem. A* **2000**, *104*, 5238.
(318) Squitieri, E.; Benjamin, I. *J. Phys. Chem. B* **2001**, *105*, 6412.
(319) Vieceli, J.; Benjamin, I. *J. Phys. Chem. B* **2002**, *106*, 7898.
(320) Zhang, X.; Walker, R. A. *Langmuir* **2001**, *17*, 4486.
(321) Zhang, X.; Esenturk, O.; Walker, R. A. *J. Am. Chem. Soc.* **2001**, *123*, 10768.
(322) Zimdars, D.; Dadap, J. I.; Eisenthal, K. B.; Heinz, T. F. *Chem. Phys. Lett.* **1999**, *301*, 112.
(323) Benderskii, A. V.; Eisenthal, K. B. *J. Phys. Chem. B* **2001**, *105*, 6698.
(324) Jarzeba, W.; Walker, G. C.; Johnson, A. E.; Kahlow, M. A.; Barbara, P. F. *J. Phys. Chem.* **1988**, *92*, 7039.
(325) Benderskii, A. V.; Eisenthal, K. B. *J. Phys. Chem. A* **2002**, *106*, 7482.
(326) Benderskii, A. V.; Henzie, J.; Basu, S.; Shang, X. M.; Eisenthal, K. B. *J. Phys. Chem. B* **2004**, *108*, 14017.
(327) Yanagimachi, M.; Tamai, N.; Masuhara, H. *Chem. Phys. Lett.* **1992**, *200*, 469.
(328) Yamashita, T.; Uchida, T.; Fukushima, T.; Teramae, N. *J. Phys. Chem. B* **2003**, *107*, 4786.
(329) Levinger, N. E. *Science* **2002**, *298*, 1722.
(330) Willard, D. M.; Riter, R. E.; Levinger, N. E. *J. Am. Chem. Soc.* **1998**, *120*, 4151.
(331) Willard, D. M.; Levinger, N. E. *J. Phys. Chem. B* **2000**, *104*, 11075.
(332) Hazra, P.; Chakrabarty, D.; Sarkar, N. *Chem. Phys. Lett.* **2003**, *371*, 553.
(333) Shirota, H.; Segawa, H. *Langmuir* **2004**, *20*, 329.
(334) Pal, S. K.; Sukul, D.; Mandal, D.; Sen, S.; Bhattacharyya, K. *Chem. Phys. Lett.* **2000**, *327*, 91.
(335) Mandal, D.; Sen, S.; Bhattacharyya, K.; Tahara, T. *Chem. Phys. Lett.* **2002**, *359*, 77.
(336) Benjamin, I. *Chem. Phys.* **1994**, *180*, 287.
(337) Michael, D.; Benjamin, I. *J. Phys. Chem.* **1995**, *99*, 16810.
(338) Michael, D.; Benjamin, I. *J. Chem. Phys.* **2001**, *114*, 2817.
(339) Vieceli, J.; Benjamin, I. *J. Phys. Chem. B* **2003**, *107*, 4801.
(340) Pantano, D. A.; Laria, D. *J. Phys. Chem. B* **2003**, *107*, 2971.
(341) Faeder, J.; Ladanyi, B. M. *J. Chem. Phys. B* **2001**, *105*, 11148.
(342) Faeder, J.; Ladanyi, B. M. *J. Phys. Chem. B* **2005**, *109*, 6732.

CR040362F